이학박사학위논문

# 표면 개질화된 전극과 뉴런 사이의 인공시냅스 전기화학에 대한 연구

Study on Electrochemistry
at Artificial Synapse between
Surface Modified Electrode and Neuron

2017 년 2 월

서울대학교 대학원
화학부 전기분석화학전공
김 은 중

A Ph. D. Dissertation

# Study on Electrochemistry at Artificial Synapse between Surface Modified Electrode and Neuron

By

Eun Joong Kim

Supervisor: Professor Taek Dong Chung

Major: Electrochemistry

Department of Chemistry

Graduate School of

Seoul National University

February 2017

# 표면 개질화된 전극과 뉴런 사이의 인공시냅스 전기화학에 대한 연구

지도교수 정 택 동

이 논문을 이학박사학위논문으로 제출함.

2017 년 2 월

서울대학교 대학원

화학부 전기분석화학전공

김 은 중

김은중의 박사학위논문을 인준함.

2017 년 1 월

위 원 장 이 연 (인)

부 위 원 장 정 택 동 (인)

위 원 민 달 희 (인)

위 원 전 누 리 (인)

위 원 김 주 훈 (인)

Abstract

# Study on Electrochemistry at Artificial Synapse between Surface Modified Electrode and Neuron

Eun Joong Kim

Department of Chemistry, Electrochemistry

The Graduate School

Seoul National University

Recently, neural interfaces such as a brain–computer interface (BCI) and reverse–engineering the brain have been actively developed along with the increasing social concerns to the brain and nerve system. The main objective of neural interface technology is to establish connections between the outside world and the nervous system, to acquire neural information or to understand neural networks. Most of neural interface techniques depend only on the

physical and passive contacts simply placing the neural electrodes near the nervous system. In the real neurobiological system, neuronal cells communicate via a chemical synapse, which is active spot where transmission of neural information in the form of action potentials (APs) and neurotransmitters occurs. Specificity of excitatory or inhibitory for the synaptic transmissions is determined by various trans-synaptic cell adhesion molecules (CAMs) that are intensively located on the membrane of neurons in the synaptic clefts. With a focus on these system of the chemical synapses, this dissertation suggests an artificial synaptic interface closely connected between electronic electrodes and neurons. Through this, it is expected that it will be able to bilaterally communicate with the synaptic-based neural information and investigate an electrochemical behavior in the artificial synapses. For construction of the artificial synaptic interface having type-specificity and durability, a series of studies were accomplished by the introduction of the engineered synaptic CAMs to the surface modification of the electrodes.

First, the robust type-specific artificial synapses were induced by artificial dendrites, which were functionalized microbeads with the engineered postsynaptic CAMs. Type-specificity of synapses, excitatory and inhibitory, regulates information process in neural networks via chemical neurotransmitters. To lay a foundation of synapse-based neural interfaces, artificial dendrites were generated by functionalizing abiotic substrata microbeads with ectodomains of

type-specific synaptogenic proteins that were C-terminally tagged with biotinylated fluorescent proteins. The excitatory artificial synapses displaying engineered ectodomains of postsynaptic neuroligin 1 (NL1-R) induced the formation of excitatory presynapses with mixed culture of neurons in various developmental stages, while the inhibitory artificial dendrites displaying engineered neuroligin 2 (NL2-R) and Slitrk3 (SL3-R) induced inhibitory presynapses only with mature neurons. By contrast, if the artificial dendrites are applied to the axonal components of micropatterned neurons, correctly-matched synaptic specificity emerges regardless of the neuronal developmental stages. The hemisynapses retained their initially established type-specificity during neuronal development and maintained their synaptic strength provided live neurons, implying the possibility of durable synapse-based biointerfaces.

Second, the artificial synapses were induced by the microelectrodes modified by electrochemically plating of gold on a commercially available MEA and immobilizing the engineered postsynaptic CAM neuroligin 1 (NL1-R). The gold electrodeplated by multi-potential pulse technique had a uniform roughness and the improved electrochemical activitiy with large surface area and low electrode impedance much more than a poly-D-lysine (PDK) coated electrode in the MEA generally used in the neuroscience field; the electrochemial depostion of Au . Because the gold electrode surface

can be also easily functionalized with biomolecules, immobilization of the biotinylated NL1-R on the electrode was facilitated after the surface modification process with biotin tagged self-assembled monolayer (SAM) reagents and streptavidins. The artificial synaptic interfaces induced on the hybrid postsynaptic microelectrodes durably maintained the type-specificity of the excitatory glutamergic by NL1-R. In addition, the postsynaptic microelectrodes would have an electrochemical activity sufficiently to *in situ* record a neural information or identify electrochemical behaviors in synaptic cleft between the electrode and the presynaptic neurons.

**Keywords:** Artificial synaptic interface, Synaptic cell adhesion molecules (CAMs), Surface modified electrode, Electrochemistry at artificial synapse

*Student number*: 2010-30091

# Contents

# List of Figures

**[Figure 2-2]** (a) Western blot profiles for the column-purified and biotinylated NL1 ectodomains. (b) The NL1 derivatives were immobilized either on supported lipid bilayer (SLB) or SAV-coated Dynabeads. (c) The membrane fluidity of bare and protein-loaded SLB was verified by fluorescence reactivation after photobleaching (FRAP) assay. Biotin-Cap-PE was mixed with egg PC as 1% (w/w) concentration, reconstituted on silica microbeads as SLB, treated with 170 nM FITC (fluorescein isothiocyanate)-coupled SAV before photobleaching within the red rectangular regions (left). After loading with R-NL1 the recovery time slightly increased (right). Left microscope images, before photobleaching; center images, right after the photobleaching; right images, after fluorescence recovery.

**[Figure 2-3]** NL1-R induces presynaptic differentiation independently of SLB membrane. (a-c) Immunocytochemistry (ICC) analysis for synaptic marker proteins in cultured hippocampal neuron. (a) NL1-R has the strongest synaptogenic activity both on SLB membrane beads and SAV Dynabeads when incubated with DIV14 hippocampal neuron culture for 2 d. (b) NL1-R shows the most prominent synaptogenic activity when immobilized on microbeads without SLB membrane. Synapsin I (Syn I) and bassoon (Bsn) aggregation were induced by PDK-coated silica beads, NL1-R on SLB, NL1-R on SAV Dynabeads. MFI = mean fluorescence intensity. Scale bar = 10 $\mu$m. ***p<0.001.

**[Figure 2-4]** NL1-R induces the formation of glutamatergic presynaptic boutons regardless of the developmental stages of cultured neurons and the incubation period. (a-h) ICC imaged for PDK-induced hemisynapses are aligned on upper lines. The cells were doubly stained either by anti-synapsin I (Syn I, red), VGluT1 (green), and VGAT (cyan). The PDK and NL1-R beads were seeded on DIV0 and incubated for 8 d (a) and 15 d (b). The beads seeded on DIV14 were incubated for 1 d (c) and 8 d (d). When seeded on DIV7, the incubation was continued for 1 d (e), 4 d (f), 3 d (g), and 15 d (h). **$p<0.01$; others $p<0.001$ between the same marker proteins.

**[Figure 2-5]** NL2-R and SL3-R induce the formation of inhibitory hemisynapses only with mature neurons. The NL2-R and SL3-R beads were seeded and analysed for the synaptogenesis as in the case of NL1-R. (a-g) ICC images for NL2-R-induced hemisynapses are aligned on upper lines. (a-d) Only excitatory presynaptic differentiations appeared during the early neuronal development stages, which lasted until DIV15. Correctly matched synapses began to appear on DIV9 when the glutamatergic specificity is still dominant (e). The fully inhibitory hemisynapses could be formed only when the artificial dendritic beads are in contact with mature neurons (DIV14) (g). **$p<0.01$; others, $p<0.001$ between the same marker proteins of NL2-R and SL3-R.

**[Figure 2-6]** Axons are compartmentalized to mimic patterned neural networks found in hippocampus. (a) Schematics showing

isolated axons in contact with excitatory (NL1-R) and inhibitory (NL2-R and SL3-R) artificial dendrites. Light image (b) and Tau-1 staining (c) shows aligned axon bundles with seeded neurons on the left and the artificial dendrites on the right. Scale bar = 20 $\mu$m. (d) The neuronal cells and the NL1-R beads were incubated for 1 d form DIV14 (d) and for 8 d form DIV7 (e) followed by the ICC analysis. n.s., not significant; others, $p<0.001$ between the same marker proteins of NL1-R, NL2-R, and SL3-R.

[Figure 2-7] Axons isolated by compartmentalized culture chamber can elicit glutamatergic presynaptic differentiation. (a) On the axonal compartment the NL1-R displaying artificial dendritic beads were seeded on DIV14 and incubated for 2 d. (b) Immunoreactivity of Tau-1, Syn I, and VGlut1. Tau-1 is an axonal marker protein. (c) The artificial dendrites near the microchannel exits exhibit stronger fluorescent puncta (red arrowheads), due to the longer co-culture period, than the ones on outgrowing axonal terminals (d). Scale bar = 15 μm.

[Figure 2-8] Synaptic specificity induced by the artificial dendrites showed little difference at near (a-c) and far from (d-f) the microchannels regardless of the seed timing of the dendritic beads. The end of the microchannels is indicated by yellow broken lines. Scale bar = 50 $\mu$m.

[Figure 2-9] Genetically engineered iGluSnFR (iESF) for in vivo biotinylation can be immobilized on streptavidin (SAV)-coated

microbeads with ease, which is used for the detection of glutamate (Glu) secreted by neurons.

**[Figure 2-10]** Glutamate (Glu) dose-response of iESF microbeads. (a) Affinity column purification of the in vivo biotinylated iESF. M, protein markers; C, cell lysate; FT, flow through; W, wash; E, elution. (b) Fluorescence images of the iESF-immobilized microbeads upon Glu input (0 - 1000 $\mu$M). (c) Titration of the iESF microsensor (n = 10 per point) with Glu using fluorescence microscopy.

**[Figure 2-11]** (a) Coincubation of the iESF microsensors and hippocampal neurons on DIV15. The SNR ($\Delta F/F$) of the iESF microsensors spread near the intertwined neurites (region S) peaked at 16.38 s after the neuronal stimulation (b, left panels and c, filled circled), whereas the sensors near the isolated neurites (region NS) showed no changes in SNR (b, right panels and c, empty circles).

**[Figure 2-12]** Excitatory hemisynapses release glutamate neurotransmitters. (a) Schematics of the measurement of glutamate spillover using engineered glutamate sensor iESF. (b) NL1-R artificial dendrites were added to the axonal compartment of DIV14 cells. After incubation for 2 d, the iESF beads were spread to the same side. Scale bar = 10 $\mu$m. (c) The neurons were stimulated by potassium shock on the somal compartment. When compared with bare SVA beads, the iESF beads near the artificial dendrites exhibited enhanced fluorescence due to the glutamate spillover.

**[Figure 3-1]** Scheme for construction of the artificial synaptic interfaces by replacing the postsynaptic neurons receiving the neural signals in the brain networks with the chemically surface modified postsynaptic electrodes.

**[Figure 3-2]** Cross-sectional schematic illustrations from the surface modification process to neuronal cell culture for construction of the artificial synaptic interfaces. (a) Structure of a generally standard MEA consisting of titanium nitride (TiN) electrode, indium tin oxide (ITO) track-lines/contact-pads, and silicon nitride (Si3N4) insulator. (b) Coating with poly-D-lysine (PDK) on the surface of TiN MEA for neuronal cell culture. (c) Electrochemically plating gold (Au) on TiN electrode coated with PDK by the potential scan or pulse techniques. (d) Formation of biotin-tagged self-assembled monolayer (SAM) (e) Immobilization of streptavidin (SAV) (f) Immobilization of the engineered postsynaptic CAM, biotinylated neuroligin 1 (NL1-R) in key factor inducing the artificial synapses. (g) Additional coating with laminin for a more stable culture condition. (f) Finally, culture of primary hippocampal neuronal cells.

**[Figure 3-3]** (a) Cyclic voltammogram for the electrodeposition and oxidation of Au on a TiN electrode coated with PDK from a solution containing 1 mM $NaAuCl_4$ and 0.2 M $NaClO_4$, at a scan rate 10 mV $s^{-1}$. The potential scan is initiated at +0.85 V (vs. Ag/AgCl) in the cathodic direction. (b) Schematic diagrams for four types of electrodeposition methods; [A] potential scan method for two

segments from +0.85 V to −0.6 V at a scan rate of 10 mV $s^{-1}$ using cyclic voltammetry technique; others using multi−potential step techniques, [B] the optimal electrodeposition potential −0.4 V with pulse duration 10 ms for 2000 cycles; [C] the same potential −0.4 V with mixed pulse duration 50 ms and 10 ms for 300 cycles and 1000 cycles, respectively; [D] a mixed pulse potential −0.4 V and 0.0 V with pulse duration 50 ms for 700 cycles.

**[Figure 3−4]** Representative microscope images of TiN electrode coated with PDK and electrochemically plated Au on the TiN electrodes by methods of four types as shown in Fig. 3−3; (a) a TiN electrode coated with PDK; others, Au plated electrodes using methods of (b) type [A], (c) type [B], (d) type [C], and (e) type [D]. (a − e, (i)) show laser reflective DIC images by confocal microscope. Scale bar = 10 $\mu$m. (a − e, (ii)) and (a − e, (iii)) show the FE−SEM images of surface and cross−section for electrodes, respectively. Scale bar = 200 nm.

**[Figure 3−5]** (a) Current response recorded by applying the potential pulse for one cycle of electroplating at −0.4 V (vs. Ag/AgCl) using 50 ms pulse duration. (b) Cyclic voltammograms for a bare TiN (black line), a TiN coated with PDK (blue line), and Au electroplated TiN electrode (red line) in a 0.5 M $H_2SO_4$ solution, at a scan rate 50 mV $s^{-1}$.

**[Figure 3−6]** Electrochemical characterizations from a bare TiN electrode to Au electroplating step by step. All data obtained in a

solution of 1 mM $K_3Fe(CN)_6$ in PBS (pH 7.0). (a, c) The voltammograms recorded by cyclic voltammetry (CV), at a scan rate 50 mV $s^{-1}$ and (b, d) the Nyquist plots recorded by electrochemical impedance spectroscopy (EIS), at the applied DC potential +0.2 V (vs. Ag/AgCl); (a, b) comparison of bare TiN and PDK coated TiN electrodes and (c, d) comparison before and after Au plating on the PDK-TiN.

**[Figure 3-7]** Electrochemical characterizations in order to confirm the electro-activity of PDK coated TiN electrode and the charge effect by PDK. Comparison of data between redox molecules with opposite charge after recorded in condition of 1 mM $K_3Fe(CN)_6$ in PBS and 1 mM $Ru(NH_3)_6Cl_3$ in PBS, respectively. (a) Normalized cyclic voltammograms at a scan rate of 50 mV $s^{-1}$. (b) Nyquist plots at the applied DC potential +0.2 V (vs. Ag/AgCl) in 1 mM $K_3Fe(CN)_6$ and the applied DC potential -0.2 V (vs. Ag/AgCl) in 1 mM $Ru(NH_3)_6Cl_3$, respectively.

**[Figure 3-8]** (a) The MEA layout; red circles indicate the position of gold (Au) electroplated electrodes. (b, c) Confocal microscope images observed after electrodeposition of Au and the surface modification with the biotinylated postsynaptic CAM, NL1-R; (b) laser reflective DIC images and (c) fluorescence images for RFP of NL1-R immobilized on the electrodes: inset images are enlarged images for one of them, respectively.

[Figure 3-9] Confirmation of electrochemical behaviors for each surface modification process for the postsynaptic electrode fabrication. All data obtained in a solution of 1 mM $K_3Fe(CN)_6$ in PBS (pH 7.0). (a) Cyclic voltammograms recorded depending on the surface modification step with a scan rate of 50 mV $s^{-1}$; Au plated PDK-TiN electrode (black), formation of biotin-SAM (blue), immobilization of streptavidin (green), immobilization of NL1-R (red), and additional coating of laminin (violet). (b) Nyquist plots of the impedance data recorded by the applied DC potential +0.2 V (vs. Ag/AgCl); Au plated PDK-TiN electrode (black), formation of biotin-SAM (blue), and finally immobilization of NL1-R (red).

[Figure 3-10] Immunocytochemistry (ICC) mages for the artificial synapses induced on the chemically modified hybrid postsynaptic electrode. (a) Merged images with DIC image and fluorescence images for antibodies of target marker proteins by confocal microscope; the arrows indicate the induced artificial synapses on the electrodes and the position of them are magnified in (b) and (c), respectively; ((i) in b, c) FE-SEM images and ((ii) in b, c) each images doubly stained by anti-synapsin I (syn I, green) and anti VGluT1 (red) and merged images by confocal microscope.

# 1. Introduction

## 1.1 Background and Overview

Brain is the most critical organ in regulation of basic functions for human life and plays an important role in control of higher-cognitive functions such as learning, memory, thinking, and emotion. Recently, social concerns to the brain and nerve system are increased beyond simply curiosity about an unexplored field. For improving the quality of life in the accelerated population ageing, many studies related to epileptic seizure or neurodegenerative diseases including Alzheimer's, Parkinson's, and amyotrophic lateral sclerosis have been actively carried out. And technological advancements have generated world-wide attentions in the neurotechnology industry involving neural engineering, neuroprosthetics, and artificial intelligence (AI). The neuroscience is rapidly advancing field and a promising playground where various techniques of other fields can be converged. The research trend related to neuroscience is extending the scope from medical devices for recording neural signals to neural interfaces sought to feedback control of neural signals.

Neural interfaces such as a brain-computer interface (BCI), sometimes called a brain-machine interface (BMI), refer to a neural

engineering area of direct communication with the nervous system using electronic devices, and involve all the range from recording the neural signals to injecting the electrical signals (stimulation) into brain [1−4]. By transducing the *in vivo* signals of neural network to electric signals of the device or vice versa, the main objective of neural interface technology is to construct a connection between the outside world and the nervous system. It is not only meaningful for assisting people with neurological sensory or motor disabilities but also for exploring the brain; to understand the structural functions of the brain and the pathway of the neural network, and to trace back to the operating principle of the brain system by the reverse engineering of the brain [5−6]. Clinically, cochlear implants and artificial retinas as representative examples of the neural interface system applying an electrical stimulation to specific sensory nerve organs have already made out success in commercialization [7]. And the deep brain stimulator (DBS) targeting the central nervous system to relieve the symptoms of Parkinson disease and dystonia is one of the most successful neural interface devices [8−10]. Technologically in the initial clinical attempt named ‘BrainGate’, it has recorded neural signals from the brain of physical disorders, and then has succeeded in moving the neuroprosthetic device using these signals [11]. Moreover, today’s noteworthy event is that the movement of the paralytic animals has been enabled by developing the feedback−controllable interface system that records electrical signals from the brain in real−time and feeds the signals to the

paralyzed part of body [8–10]. In accordance with these flows, various neural electrodes made with electrically active materials and effective forms have been consistently developed and reported for studying the ideal neural interface. The neural electrode can be classified into two types according to applications. The implantable invasive electrodes such as platform array (Utah array), multisite probe (Michigan electrode), and microwires are typical for in vivo brain study [12–15]. And for in vitro research on neural tissue or cultured neuronal cells, there are commercialized microelectrode arrays (MEAs) and various types of electrodes reported such as improved gold MEAs, silicon nanowires, carbon nanotubes, and conducting polymer nanotubes [16–23]. Although these outcomes of the devices and electrodes have appreciably reached a certain level, the problem of methodological limitations has still remained. The existing techniques discussed so far are passive systems that rely entirely on an indirectly physical contact between the electronics and the nervous system, and have been focused on the detection of electrical neural signals such as electroencephalograms (EEGs), electrocorticograms (ECoGs), local field potentials (LFPs), or action potentials (APs) [24–28]. It has difficulties in acquiring the information at the level of single neurons in brain, or understanding a comprehensive information exchange on real neural networks. In addition, since the selectivity for the types and regions of neurons may be insufficient, a level of decoding the neural information can be extremely naive and limited. However, the neural information

network within the actual brain is achieved by a parallel communication of much more complex and diverse signals. Therefore, in order to grasp the ultimate meaning of the communication between neurons, it is necessary to understand the structure of nerve cells and their signaling system.

In the real nervous system, neuronal cells communicate via synapse, which is cellular gap junction by intercellular connection between adjacent neurons. The synapse is active spot where transmission of neural information thereby converting electrical signals, called by action potential (AP), into neurotransmitters as chemical messenger. Neurotransmission at the chemical synapse relies on the exocytosis of synaptic vesicles containing neurotransmitters and results in the generation of a postsynaptic electrical signal derived from a presynaptic electrical signal; the neurotransmitters released into synaptic cleft are crucial determinants of whether or not to transmit the presynaptic information to the postsynaptic neurons. By controlling the frequency and intensity of the neurotransmission through these synapses (synaptic plasticity), neurons form an interconnected synaptic network, which is an important basis for major cognitive functions such as learning and memory. The functional synaptic clefts are very narrow space about tens to hundreds of nanometers between axons of presynaptic neuron and dendrites of postsynaptic neuron (Fig. 1-1a). Various trans-synaptic cell adhesion molecules (CAMs) are

located on the plasma membrane of neurons and interconnected with particular pairs in the clefts (Fig. 1-1b). They play a significant role in determining specificity of the synaptic transmissions; excitatory synapses that activate the signaling to postsynaptic neurons, or inhibitory synapses that block it [29]. However, without considering the system of such a chemical synapse, a general information processing in the field of neural interfaces depends exclusively on passive physical contact between nerve cells and non-biological electronic devices. Therefore, in stepping with the research trend of neural interface, there have been many attempts to mimic the brain's system, and researchers interested in this area are mainly focusing on the chemical synapse. They reported several concepts that have been called artificial synapses; a system of microfluidic chip containing a separate neurotransmitter channel under the neuronal cell culture side [30-31], co-culture system of neurons and microbeads coated with positive charged poly-D-lysine (PDL) [32] or supported lipid bilayers (SLBs) containing cationic lipids [33], and further results of micro-patterned substrates applied with immobilizing synaptic CAMs [34-35]. Although these achievements may have succeeded in artificially inducing or structurally mimicking synapses, it is not application system of the neural interface that reads or transmits meaningful signals through synapses. The achievements also can have a great impact on the fundamental understanding of synaptic systems as well as the development of applications such as therapeutics or neuroprosthetics, however it is

difficult to explore the synaptic cleft in which electrical and chemical behaviors occur.

As a new approaching strategy unlike with such the existing system in the field of neural interface, this dissertation regards the synaptic cleft as a bio-hybrid nanogap to study the electrochemical behaviors, and focuses on the artificial synaptic interfaces for bilateral communications that can be a feedback-control. The artificial synaptic interface research began with the idea of providing a much more sophisticated interface; that is closely connected between electronic devices and neurons, and then can distinguish the excitatory and inhibitory signals in the synapse-based meaningful information. This thesis is divided into two main sections. In Chapter 2, we discuss the durable type-specific hemisynapses artificially induced by using the microbeads immobilized with the engineered postsynaptic CAMs. Among the well-known postsynaptic CAMs, ectodomains of neuroligin 1 (NL1), neuroligin 2 (NL2), and Slitrk3 (SL3), are C-terminally tagged with biotinylated fluorescent proteins. The microbeads immobilized with the engineered postsynaptic CAMs named as artificial dendrites induce type-specific presynaptic differentiation (excitatory or inhibitory) into contacted neurons; the induced artificial hemisynapses are very robust, and have selective functions depending on the type of the synaptic CAMs. And in Chapter 3, we discuss the efforts focused on replacing the postsynaptic neurons that receive the signals in neural

networks with the modified electrodes for constructing the artificial synaptic interface, based on the results of Chapter 2. Techniques of the surface modification for fabricating the hybrid postsynaptic electrodes capable of inducing artificial synapses and recording neural signals are mainly mentioned; we perform an electrochemical deposition of gold (Au) on the commercialized MEA (TiN MEA) made of titanium nitride, and then modify the Au-TiN MEA with the biotinylated NL1-R. The modified MEA, that are the hybrid postsynaptic microelectrodes, is electrochemically active enough to be applied as a neural recording electrode, and induces the glutamatergic artificial synapse by contacting with the cultured primary neurons. We are continuously working to detect the electrical or chemical signals of neuron via the artificial synaptic interface formed on the postsynaptic electrode, and the research on this part is ongoing.

a

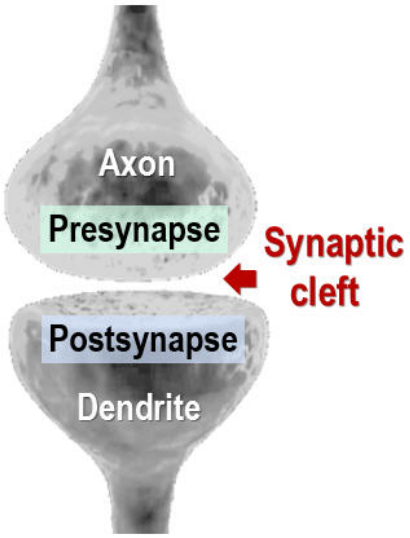


b

| Cell adhesion molecules (CAMs) | | Specificity | |
|---|---|---|---|
| Presynaptic | Postsynaptic | Excitatory | Inhibitory |
| β-Nrx | NL1 | ○ | |
| α-Nrx | NL2 | ○ | ○ |
| PTPδ | Slitrk3 | | ○ |
| LAR-RPTP | Slitrk4 | ○ | |
| Netrin-G1 | NGL1 | ○ | |
| Netrin-G2 | NGL2 | ○ | |
| LAR-RPTP | NGL3 | ○ | |
| β-Nrx | LRRTM2 | ○ | |

Nrx; Neurexin
NL; Neuroligin
Slitrk; Slit and neurotrophic receptor tyrosine kinases-like family member
PTP; Protein tyrosine phosphatase
LAR-RPTP; Leukocyte antigen-related receptor protein tyrosine phosphatase
NGL; Netrin G ligand
LRRTM; Leucine rich repeat transmembrane

**Fig. 1-1** (a) Schematic structure of the synapse. Synaptic cleft, a nanogap between pre- and postsynaptic neuron, is a major playground of neurotransmitters. (b) Various trans-synaptic cell adhesion molecules (CAMs) determine excitatory and inhibitory subtype specificity.

## 1.2 References


[1] A. B. Schwartz, X. T. Cui, D. J. Weber and D. W. Moran, *Neuron*, 2006, *52*, 205.

[2] A. B. Schwartz, *Annu. Rev. Neurosci.*, 2004, *24*, 487.

[3] M. A. Lebedev and M. A. L. Nicolelis, *Trends Neurosci.*, 2006, *29*, 536.

[4] J. D. Wander and R. P. Rao, *Curr Opin Neurobiol.*, 2014, *25*, 70

[5] E. Hahn, *IEEE Spectrum*, 2008, 51.

[6] G. Cauwenberghs, *Proc. Natl. Acad. Sci.*, 2013, *110*, 15512

[7] W. F. House, *Ann. Otol. Rhinol. Laryngol.*, 1976, *83*.

[8] V. Gradinaru, M. Mogri, K. R. Thompson, J. M. Henderson and K. Deisseroth, *Science*, 2009, *324*, 354.

[9] C. T. Moritz, S. I. Perlmutterm and E. E. Fetz, *Nature*, 2008, *456*, 639.

[10] A. Jackson, J. Mavoori, E. E. Fetz, *Nature*, 2006, *444*, 56.

[11] R. A. Normann, *Nat. Clin. Pract. Neuro.*, 2007, *3*, 444.

[12] D. R. Kipke, W. Shain, G. Buzsaki, E. Fetz, J. M. Henderson, J. F. Hetke and G. Schalk, *J. Neurosci.*, 2008, *28*, 11830.

[13] M. R. Abidian and D. C. Martin, *Biomaterials*, 2008, *29*, 1273.

[14] L. R. Hochberg, M. D. Serruya, G. M. Friehs, J. A. Mukand, M. Saleh, A. H. Caplan, A. Branner, D. Chen, R. D. Penn and J. P. Donoghue, *Nature*, 2006, *442*, 164.

[15] S. Negi, R. Bhandari, L. Rieth, R. Van Wagenen and F. Solzbacher, *J. Neurosci. Methods*, 2010, *186*, 8.

[16] A. Hai, J. Shappir and M. E. Spira, *Nat. Methods*, 2010, *7*, 200.

[17] M. E. Spira and A. Hai, *Nat. Nanotechnol.*, 2013, *8*, 83.

[18] D. B. Suyatin, L. Wallman, J. Thelin, C. N. Prinz, H. Jorntell, L. Samuelson, L. Montelius and J. Schouenborg, *Plos One*, 2013, *8*, e56673.

[19] X. J. Duan, R. X. Gao, P. Xie , T. Cohen-Karni, Q. Qing, H. S. Choe, B. Z. Tian, X. C. Jiang and C. M. Lieber, *Nat. Nanotechnol*,. 2012, *7*, 174.

[20] W. Hallstrom, T. Martensson, C. Prinz, P. Gustavsson, L. Montelius, L. Samuelson and M. Kanje, *Nano Lett.*, 2007, *7*, 2960.

[21] B. Z. Tian, T. Cohen-Karni, Q. Qing, X. J. Duan, P. Xie, C. M. Liebe, *Science*, 2010, *329*, 830.

[22] J. T. Robinson, M. Jorgolli, A. K. Shalek, M. H. Yoon, R. S. Gertner, H. Park, *Nat. Nanotechnol.*, 2012, *7*, 180.

[23] M. R. Abidian, K. A. Ludwig, T. C. Marzullo, D. C. Martin, D. R. Kipke, *Adv. Mater.*, 2009, *21*, 3764.

[24] P. Fattahi, G. Yang, G. Kim and M. R. Abidian, *Adv. Mater.*, 2014, *26*, 1846.

[25] J. R. Wolpaw, N. Birbaumer, D. J. McFarland, G. Pfurtscheller and T. M. Vaughan, *Clin. Neurophysiol.*, 2002, *113*, 767.

[26] M. A. Lebedev and M. A. L. Nicolelis, *Trends Neurosci.*, 2006, *29*, 536.

[27] J. R. Wolpaw and D. J. McFarland, *Proc. Natl. Acad. Sci.* 2004, *101*, 17849.

[28] L. R. Hochberg, D. Bacher, B. Jarosiewicz, N. Y. Masse, J. D. Simeral, J. Vogel, S. Haddadin, J. Liu, S. S. Cash, P. van der Smagt and J. P. Donoghue, *Nature*, 2012, *485*, 372.

[29] M. B. Dalva, A. C. McClelland and M. S. Kayser, *Nat. Rev. Neurosci.*, 2007, *8*, 206.

[30] M. C. Peterman, J. Noolandi, M. S. Blumenkranz and H. A. Fishman, *Proc. Natl. Acad. Sci.*, 2004, *101*, 9951.

[31] D. S. Jeong, I. Kim, M. Ziegler and H. Kohlstedt, *RSC Adv.*, 2013, *3*, 3169.

[32] A. L. Lucido, F. S. Sanchez, P. Thostrup, A. V. Kwiatkowski, S. L.-Ortiz, G. Gopalakrishnan, D. Liazoghli, W. Belkaid, R. B. Lennox, P. Grutter, C. C. Garner and D. R. Colman, *J. Neurosci.*, 2009, *29*, 12449.

[33] A. L. Lucido, G. Gopalakrishnan, P. T. Yam, D. R. Colman and R. B. Lennox, *ACS Chem. Neurosci*,. 2010, *1*, 535.

[34] P. Shi, M. A. Scott, B. Ghosh, D. Wan, Z. Wissner-Gross, R. Mazitschek, S. J. Haggarty and M. F. Yanik, *Nat. Commun.*, 2011, *2*, 510.

[35] K. Czondor, M. Garcia, A. Argento, A. Constals, C. Breillat, B. Tessier and O. Thoumine, *Nat. Commun.*. 2013, *4*, 2252.

# Part 1.

## Robust Type-Specific Artificial Synapses Induced by Artificial Dendrites

# 2. Robust Type-Specific Artificial Synapses Induced by Artificial Dendrites

## 2.1 Introduction

In neurobiological systems, the communication between neurons is dynamically generated through a chemical synapse whose gap is interconnected with a variety of trans-synaptic cell adhesion molecules (CAMs) that specify the excitatory and inhibitory properties [1]. At the presynapses, the electrical signals, called action potentials (APs), are converted into chemical signals mediated by neurotransmitters that either excite or inhibit postsynaptic APs depending upon the types of the chemical synapses. Consequently, a sophisticated regulation of excitatory and inhibitory signals is crucial for the constitution of functional neuronal networks [2]. Such complexity of brain nervous system makes it difficult to reconstitute broken neuronal pathways or damaged part of the brain [3-4].

One of the most striking features in synaptogenesis is that neurons can form 'hemisynapses' with a non-biological partner whose surface is covered with functional synaptic CAMs [5-7]. Such hemisynapses garner much attention because they can secure the connection between the two heterologous systems with defined geometry [8-10]. However, there has been lack of information about

the dependency of neuronal morphology on synaptic specificity, the durability of excitatory and inhibitory hemisynapses, and the methodology of synaptic CAM engineering for the generation of robust artificial dendrites that enable the formation of type-specific hemisynapses.

Among the trans-synaptic interactions between the synaptic CAMs, the adhesion between postsynaptic neuroligins (NLs) and presynaptic neurexins (Nrxs) plays pivotal roles in synapse formation, differentiation and validation [11]. The excitatory (glutamatergic) presynaptic differentiation is induced by NL1, 3 and 4, and the inhibitory (GABAergic) by NL2 [12-15]. While many other synaptic CAMs and their roles are rapidly emerging, only Slitrk3-PTP$\delta$ pair has shown an unprecedented specificity to inhibitory synapses [16-18]. Using the synaptic CAMs, synapse-based neural networks have been developed by compartmentalized co-culture of neuronal cells with heterogeneous cell lines [19-23], primary neuron culture on micropatterned substrates on which purified synaptogenic proteins are immobilized [7,24]. Such microfabricated neural networks are useful for fundamental and therapeutic studies of synaptic systems, including reformation of functional synapses and high-throughput screening of small molecules and proteins that affect synaptogenesis. To reconstitute the broken neuronal networks in the brain or body parts, however, three fundamental issues should be addressed beforehand: the sub-type specificity, durability and spatiotemporal regulation of the

artificial synapses. Although the purified synaptic CAMs have been used to induce the formation of type-specific hemisynapses [5,7,25], there has been lack of information as to how long the hemisynapses last and when the specificity consolidates.

Herein, we reconstituted durable inhibitory and excitatory hemisynapses with spatiotemporal regulation using type-specific artificial dendrites that display modularly-tagged ectodomains of postsynaptic CAMs, such as NL1, NL2, and Slitrk3; by engineering the postsynaptic CAMs with biotinylation, high density and strength of immobilization on the surface of solid substrate are guaranteed. We found that in random culture of hippocampal neurons the artificial dendrites can form correctly-matched hemisynapses with fully developed neurons, whereas with immature neurons only excitatory hemisynapses. Remarkably, in micropatterned culture of neurons mimicking aligned neural networks in the hippocampus, the artificial dendrites can form correctly-matched hemisynapses with isolated axonal components of immature neurons. Furthermore, the synaptic strength and the type-specificity of the hemisynapses, once established, remained unchanged as long as live cells are provided.

## 2.2 Experimental Methods

### 2.2.1 Reagents and materials

Poly-D-lysine (PDK, Mw 70,000-150,000, P08990), bovine serum albumin (BSA, A3059), streptavidin (85878), Triton X-100 (X100) and ethanol were purchased from sigma. Silica beads (2.56 and 5 $\mu$m in diameter) were from Bangs Laboratories Inc. Egg phosphatidylcholine (PC) and 1,2-dipalmitoyl-*sn*-glycero-3-phophoethanolamine-*N*-(cap-biotinyl) (sodium salt) (Biotin-Cap-PE) were form Avanti Polar Lipids. Dynabeads M-280 Streptavidin (2.8 $\mu$m in diameter) was purchased from Invitrogen. Dulbecco's Phosphate Buffered Saline (DPBS, LB001-02) and DPBS containing $CaCl_2$ (LB001-04) were from Welgene. Silicon wafer (4-in in diameter) was purchased from Silicon Inc. and photoresists, SU-8 5 and SU-8 50 were from Microchem. Poly(dimethylsiloxane) (PDMS, Sylgard 184) was purchased from Dow Corning and propyleneglycolmethylether acetate (PGMEA) photoresist developer (537543) was used. Paraformaldehyde (P2031) was from Biosesang and normal donkey serum (017-000-121) was purchased from Jackson ImmunoResearch Inc. Rabbit synapsin I (Syn I) polyclonal antibody (AB1543), guinea pig vesicular glutamate transporter 1 (VGluT1) polyclonal antibody (AB5905), Mouse tau-1 monoclonal antibody (MAB3420), and rabbit vesicular GABA transporter (VGAT) polyclonal antibody (AB5062P) were from Millipore. Mouse synapsin

I monoclonal antibody (106 001) and rabbit VGluT1 polyclonal antibody (135 303) were from Synaptic Systems. Mouse bassoon monoclonal antibody (ab82958) was purchased from Abcam. Secondary antibodies conjugated with Alexa Fluor 405, 488 and 633 were from Invitrogen. 18 MΩ · cm deionized water produced by Barnstead NANOpure (Thermo Scientific Inc.) was used to prepare all the solutions.

### 2.2.2 Preparation of PDK-coated microbeads

Silica microbeads (2.56 and 5.06 $\mu$m in diameter, $3 \times 10^5$ beads) were incubated with PDK solutions (0.5 mg/mL in DPBS) for overnight at room temperature, washed with DPBS for three times, and spread on cultured neuronal cells per condition. For the co-incubation with the synaptic CAMs-microbeads, that is to say artificial dendrites, $0.5 \times 10^5$ beads were spread. Otherwise, $1.0 \times 10^5$ beads were used to examine the formation of the PDK hemi-synapse [10].

### 2.2.3 Preparation and quantification of synaptic CAMs immobilized on SLBs microbeads

Chloroform lipid solutions of Egg PC and Biotin-Cap-PE were mixed (99 mol% Egg PC and 1 mol% Biotin-Cap-PE), dried under a stream of nitrogen followed by desiccation under vacuum for overnight, and then hydrated in filter-sterilized DPBS to yield 5

mg/mL initial concentrations of phospholipids. For preparation of small unilamellar vesicles (SUVs), the lipid solutions were sonicated for 1 h and extruded more than eleven times through polycarbonate filters with 50 nm pores [6]. Then, the solution of SUVs was diluted in DPBS to a final concentration of 1 mg/mL and incubated with silica microbeads (5.06 $\mu$m in diameter, $3 \times 10^5$ beads) for 30 min at room temperature. Supported lipid bilayers (SLB) were formed by the fusion of SUVs on the silica beads. After rinsing, the SLB-beads were incubated with DPBS containing BSA (100 $\mu$g/mL) for 45 min at room temperature. The beads were washed with DPBS, then streptavidin (SAV) was added, followed by incubation for 60 min. The SAV immobilized SLB-beads were rinsed, and incubated with the biotinylated synaptic CAMs solution for overnight. After rinsing with DPBS, $1.0 \times 10^5$ beads were added to cultured neuron. For the co-incubation with the other microbeads, that are PDK coated microbeads or synaptic CAMs immobilized SLB-beads, $0.5 \times 10^5$ beads were spread.

### 2.2.4 Preparation of synaptic CAMs immobilized on Dynabeads

Dynabeads M-280 streptavidin stock solution ($6.0-7.0 \times 10^5$ beads/$\mu$L) was added to the biotinylated synaptic CAMs solutions and incubated for overnight at room temperature. After rinsing with DPBS, the synaptic CAMs coated Dynabeads were prepared to a final

density of 3.0 × $10^5$ beads, and 1.0 × $10^5$ beads were added to cultured neuronal cells per conditions. For the co-incubation with the other microbeads, that are PDK coated microbeads or synaptic CAMs immobilized SLB-beads, 0.5 × $10^5$ beads were spread.

### 2.2.5 Fabrication of microfluidic culture chamber for axonal compartmentalization

To make preparation of microfluidic chambers, we used photoresists using photolithography and PDMS materials using soft lithography and replica molding. First, we fabricated master patterns on a cleaned 6-inch silicon (Si) wafer using two layers of negative photoresist SU-8 5 (3 $\mu$m thickness, 10 $\mu$m width, and 900 $\mu$m length) and SU-8 50 (100 $\mu$m thickness, 1.5 mm width, and 7 mm length) on a silicon wafer; to be microgrooves (microchannels) and the cell culture compartments (somal chamber and axonal chamber) [28-29]. Second, the patterned Si wafer was placed in Petri dish, cast in a PDMS prepolymer mixture (10:1 ratio) of Sylgard 184, and then cured in a laboratory oven at 70 ° C for 3 h. The solidified PDMS containing desired patterns (the approximate size of 2 cm × 2 cm) was cut out and separated from the master mold. Until used, the PDMS piece was stored in 70% ethanol for sterilization. Finally, we washed the PDMS chamber from ethanol using pure DI water. After washing, the chambers were completely dried in clean bench (laminar flow hood) and reversibly bonded on the PDK-coated coverslips. We

filled the assembled culture chamber with sterilized DI water, then replaced with plating media for at least 2–3 h before seeding the neuronal cells.

### 2.2.6 Primary culture of rat hippocampal neuronal cells

Protocols were approved by the Institutional Animal Care and Use Committee (IACUC) of Seoul National University. Primary rat hippocampal neuronal cells were obtained from Sprague–Dawley (SD) rat embryos at day 18 of gestation (E18). Briefly, hippocampus dissected from E18 rat embryos were rinsed with HBSS (Hanks' Balanced Salt Solution), and incubated with papain and DNase with 60 rpm for 30 min at 37 ° C. After rinsing with solution of 10% and 5% FBS (fetal bovine serum) in HBSS, sequentially. Individual single cells were mechanically isolated by trituration about 10 times in 2 mL HBSS containing DNase with silanized Pasteur pipette, which the pipette tip was barely polished with fire. The cell suspension was diluted to density of $2 \times 10^5$ cells/mL with plating media containing MEM supplemented with 0.6% (v/v) glucose, 10 mM sodium pyruvate, 1 mg/mL FBS, 1% Penicillin–Streptomycin, and 100 $\mu$g/mL Primocin. Then, the media solution with cells plated on the PDK–coated coverslips placed in Petri dish (finally seeding density of 200 cells/mm$^2$ on the coverslips). For culture on the microfluidic culture chamber unlike the above culture condition, the cell suspension was diluted to density of $3 \times 10^6$ cells/mL with the plating media, and then

plated on the only one side of the chamber (the somal side) with 50 $\mu$L of the media containing the cells. After 3 h the cell culture media was exchanged with neurobasal medium supplemented with B27 containing 2 mM glutamax. Cultures were maintained in an incubator at 37 ° C and 5% $CO_2$ atmosphere, and on changing the medium every 3-4 days.

### 2.2.7 Sensing of glutamate released on induced artificial synapses

For the measurement of glutamate spillover, we engineered the intensity-based glutamate-sensing fluorescent reporter (iGluSnFR) [30], dubbed 'iESF', to directly measure the rapid glutamate transients. The engineered and purified iESF has the sensitivity enough for our experiments [31]. The purified iESF (1.5 mg/mL) was incubated with Dynabeads M-280 streptavidin suspension at 25 ° C until saturation. The iESF-beads were magnetically separated from the solution, briefly washed, and re-suspended in DPBS before use.

When primary hippocampal neuronal cells were cultured at 15 DIV, the culture medium was exchanged with DPBS containing $CaCl_2$ before loading the iESF-beads ($3 \times 10^5$ beads) to cells. After incubation for 10 min fluorescence images were captured by fluorescence microscope (Eclipse Ti-E, Nikon) with excitation/emission at 485/515 nm wavelength at 4.8 frame per

second (fps) for ~1 min, during which the neurons were stimulated by applying a final concentration of 200 mM KCl in DPBS. Similarly, sensing of glutamate released on the induced artificial synapses was performed in accordance with above process; capturing fluorescence images of iESF-beads in the axonal side of the culture chamber during stimulated the neuronal cells in the somal side of the chamber.

### 2.2.8 Immunocytochemistry (ICC)

Neuronal cells were fixed using 4% para-formaldehyde for 25 min and rinsed once with DPBS and two times with Tris-buffered saline (TBS, pH 7.4). The cells were then incubated in blocking solution, containing 4% BSA and 0.1% Triton X-100, dissolved in TBS for 30 min, followed by incubation in primary antibodies diluted in TBS containing 0.5% BSA and 0.1% Triton X-100 for overnight at 4 ° C. The samples were then washed three times with TBS and the fluorescent secondary antibodies were applied for 1 h at room temperature in TBS containing 0.5% BSA. The samples were washed again three times with TBS and once with filter-sterilized DDW, and stored in VECTASHIELD Mounting Medium at -80 ° C until microscopic examination. Fluorescence images were taken with a Zeiss LSM710 confocal laser scanning microscope equipped with ZEN2009 software at the National Centre for Inter-university Research Facilities (NCIRF) at Seoul National University.

### 2.2.9 Image quantification and analysis

To reflect both the frequency of synaptogenesis and the intensity of the hemi-synapses formed by the artificial dendrites, at least 30 beads were randomly chosen as regions of interest (ROI) from the DIC (differential interference contrast) image by excluding somal regions per condition per experiment using NIS-Elements AR software (Nikon). The same-sized ROI with the similar neurite density and without the bead was set as control. The ROI profiles were applied to each fluorescence channel and the mean fluorescence intensity (MFI) was collected by NIS-Elements AR software. For the time-dependent experiments (Fig. 2-4 and Fig. 2-5), the MFI values of each channel was separately normalized to the maximum MFI values of the respective marker proteins. For the time- and compartment-dependent experiment using micropatterned neurons (Fig. 2-6), the overall MFI values of VGluT1 and VGAT were first normalized to the ones of Syn I, followed by the individual normalization to the maximum MFI values of the respective marker proteins.

For determination of glutamate released on the induced artificial synapses, the standard titration curve was obtained in DPBS with 200 ms exposure time corresponding to 4.8 fps beforehand. The fluorescence images were analysed by NIS-Element AR software (Nikon) where at least ten ROI were selected for MFI calculation. After the fluorescence measurements, changes in fluorescence intensity of the ROIs were calculated as $\Delta F/F$, where F is the average

baseline fluorescence and $\Delta F$ is the fluorescence intensity at glutamate input minus the baseline fluorescence ($\Delta F/F = (F_{glutamate} - F_0) / F_0$). All images were prepared for figure using Photoshop (Adobe).

### 2.2.10 Statistics

All statistics were performed using Origin 8.0 software. For comparisons of MFI between multi-group datasets, we carried out one-way ANOVA with Bonferroni's method. All data shown are mean ± SEM (standard error of the mean). In figures, statistical significance is indicated by n.s. for $p > 0.05$, * for $0.05 > p > 0.01$, ** for $0.01 > p > 0.001$, and *** for $p < 0.001$.

## 2.3 Results and Discussion

### 2.3.1 Modularly tagged synaptic CAM ectodomains

To generate type-specific artificial dendrites, ectodomains of NL1 (48-639), NL2 (15-614), and Slitrk3 (28-649) were excerpted from their full sequences. NL1 ectodomain was determined by the minimally secreted functional domain [30] and the crystal structure that reveals Leu636 as the end of the $\alpha$-helix required for NL1 dimerization [31-32] that induces presynaptic differentiation via clustering of presynaptic neurexins (Nrxs). Ectodomain of NL2 (15-614) was determined by sequence comparison with NL1. The Slitrk3 ectodomain contains two leucine-rich repeat domains (LRR1 and LRR2) followed by several extra C-terminal residues. To facilitate massive production, purification, quantification, and localization of the ectodomains, we designed a tagging module that can be generally applied to virtually all kinds of synaptic CAM ectodomains. We began by engineering the NL1 ectodomain by placing YFP or RFP either at the N- or C-terminus of the protein and a biotin acceptor peptide (AP, also called AviTag) [33] at the end of the expression cassette to utilize biotin-streptavidin (SAV) interaction for immobilization of the protein (Fig. 2-1 and Fig. 2-2a,b). The *in vivo* biotinylation was further simplified by bicistronic expression of endoplasmic reticulum-specific bacterial biotin ligase (BirA-ER) (Fig. 2-1b).

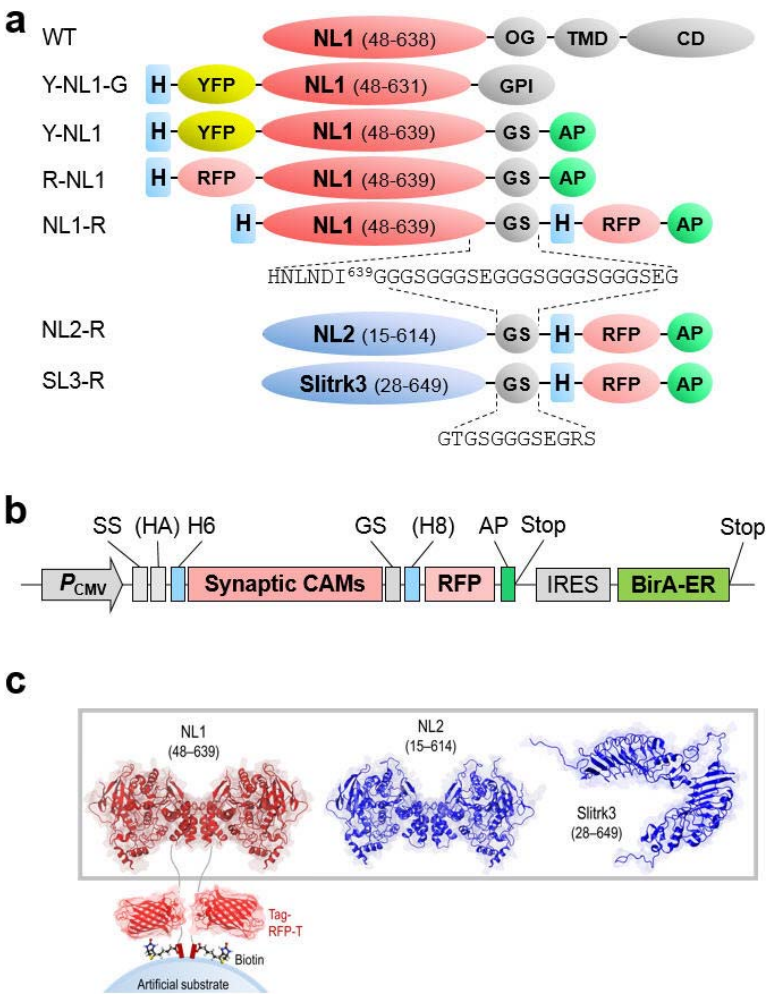


**Fig. 2-1** (a) Comparison of domain structures of engineered ectodomain of postsynaptic CAMs. WT, wild type; YFP, yellow fluorescent protein; RFP, red fluorescent protein (TagRFP-T); H, hexa- or octa-His tag; OG, O-glycosylation rich domain; TMD, transmembrane domain; CD, cytoplasmic domain; GPI, glycosylphosphatidylinositol anchoring motif; GS, glycine-serine linker; AP, biotin acceptor peptide (AviTag). (b) Structure of optimized expression vector. Bicistronic Expression of BirA for mass production of *in vivo* biotinylated postsynaptic CAMs. SS, signal sequence; HA, hemagglutinin affinity tag; H6, hexa-His tag; H8, octa-His tag; IRES, internal ribosome entry site. The SS, HA and H6 can vary depending upon the type of the postsynaptic CAMs. (c) Schematic structure of excitatory and inhibitory artificial dendrites displaying C-terminally tagged ectodomains of postsynaptic NL1 (NL1-R), NL2 (NL2-R) and Slitrk3 (SL3-R).

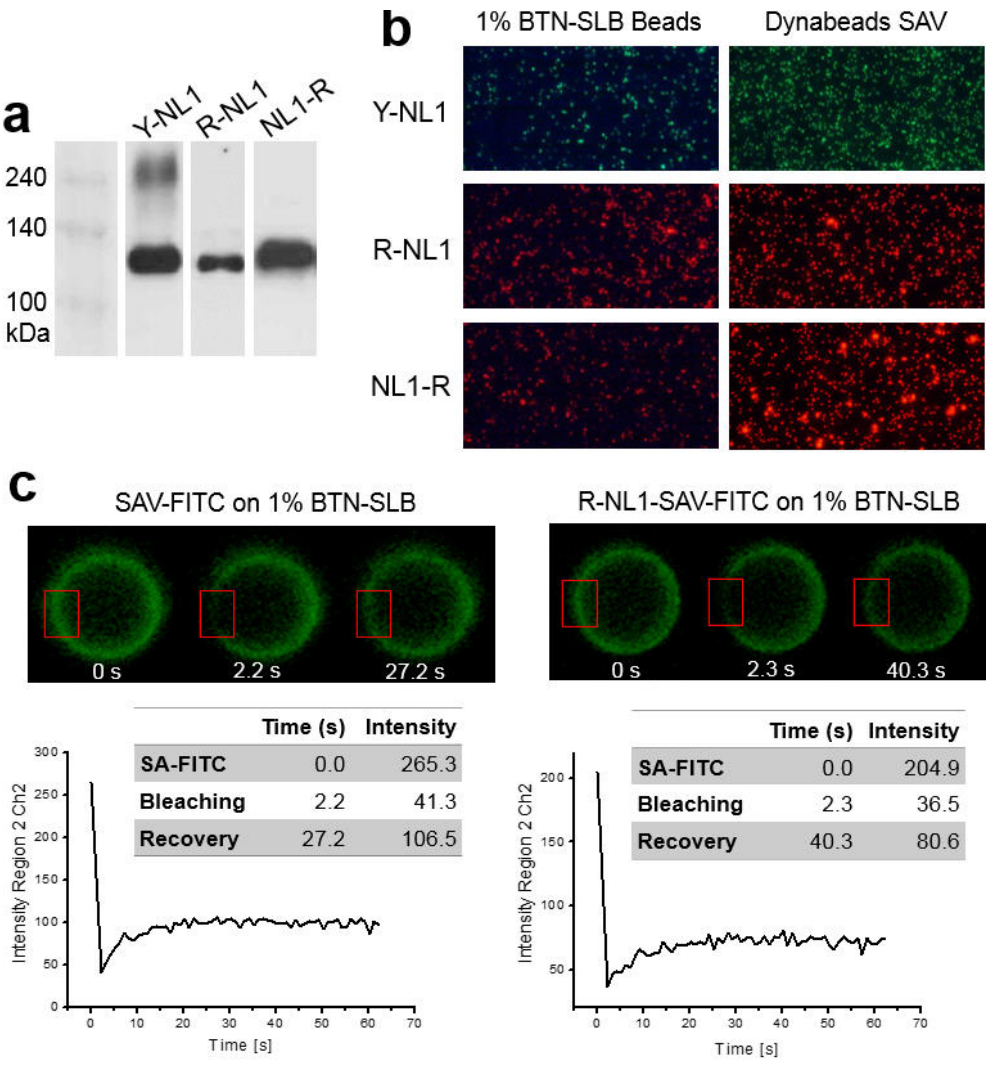


**Fig. 2-2** (a) Western blot profiles for the column-purified and biotinylated NL1 ectodomains. (b) The NL1 derivatives were immobilized either on supported lipid bilayer (SLB) or SAV-coated Dynabeads. (c) The membrane fluidity of bare and protein-loaded SLB was verified by fluorescence reactivation after photobleaching (FRAP) assay. Biotin-Cap-PE was mixed with egg PC as 1% (w/w) concentration, reconstituted on silica microbeads as SLB, treated with 170 nM FITC (fluorescein isothiocyanate)-coupled SAV before photobleaching within the red rectangular regions (left). After loading with R-NL1 the recovery time slightly increased (right). Left microscope images, before photobleaching; center images, right after the photobleaching; right images, after fluorescence recovery.

### 2.3.2 Optimal structure for C-terminally tagged NL1 ectodomain function *in vitro*

Although the previously reported excitatory hemisynapses were induced by NL1 ectodomain docked on obligate supported lipid bilayer (SLB) membrane [5,6], obviating the lipid layer should simplify the fabrication process of the artificial dendrites and greatly extend the types of surface on which synaptic proteins are immobilized. In addition, we can minimize a hindrance to communication, if possible, between neurons and the artificial dendrites. When we compared the synaptogenic activity of the N- or C-terminally-tagged NL1 ectodomains immobilized on SAV-coated microbeads (Dynabeads M-280 Streptavidin, 2.8 $\mu$m in diameter) and silica microbeads (5 $\mu$m in diameter) covered with SAV-loaded fluidic SLB membrane (Fig. 2-2c), only C-terminally tagged NL1-R immobilized without lipid layer showed the most prominent synaptogenic activity by showing aggregated synapsin I, a general synapse marker protein (Fig. 2-3). The synaptogenic potential of NL1-R was greater than the one of poly-D-lysine (PDK) that is also known to induce the formation of synaptic boutons with mature neurons [10,34-35]. We then applied the same tagging module to the inhibitory NL2 and Slitrk3 ectodomains to establish a complementary type-specificity, generating NL2-R and SL3-R (Fig. 2-1a).

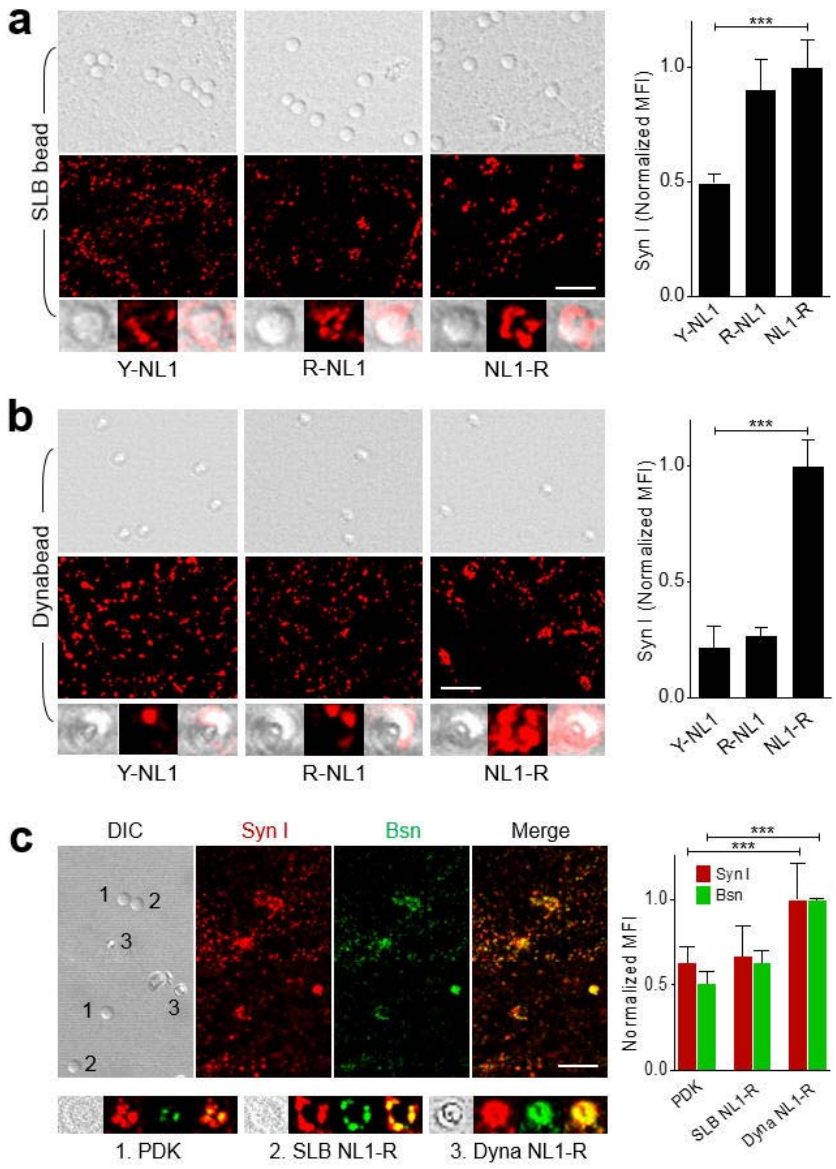


**Fig 2-3** NL1-R induces presynaptic differentiation independently of SLB membrane. (a-c) Immunocytochemistry (ICC) analysis for synaptic marker proteins in cultured hippocampal neuron. (a) NL1-R has the strongest synaptogenic activity both on SLB membrane beads and SAV Dynabeads when incubated with DIV14 hippocampal neuron culture for 2 d. (b) NL1-R shows the most prominent synaptogenic activity when immobilized on microbeads without SLB membrane. Synapsin I (Syn I) and bassoon (Bsn) aggregation were induced by PDK-coated silica beads, NL1-R on SLB, NL1-R on SAV Dynabeads. MFI = mean fluorescence intensity. Scale bar = 10 $\mu$m. ***p<0.001.

### 2.3.3 Durable glutamatergic presynaptic differentiation induced by NL1-R

The PDK-coated beads serve as synaptogenic substrates only when they are introduced to dissociated hippocampal cells after a certain developmental stage (at least DIV7) [10]. The PDK-induced hemisynapses, instructed by F-actin reorganization and heparan sulfate proteoglycans (HSPGs), increased after 24 h incubation and could be observed up to 72 h [10]. Unfortunately, they lack synapse specificity, inducing the formation of both excitatory and inhibitory synaptic boutons. Postsynaptic NL1, on the other hand, is a negatively charged protein that specifically binds to $\beta$-Nrx expressed on the outgrowing axonal surface, thereby regulating the synapse specificity. However, synaptic CAMs can induce the formation of mismatched synapses between glutamatergic and GABAergic synaptic terminals in the early developmental stages [34-36]. We thus examined the synaptic specificity of the NL1-coated artificial dendrites by seeding them to a mixed culture of neurons in various developmental stages. When we seeded the PDK and NL1-R beads from the beginning of the neuron culture (DIV0) and incubated up to DIV8 and 15, we found that in both durations only the NL1-R-coated beads successfully induced excitatory presynaptic differentiation, showing immunoreactivity toward synapsin I and VGluT1, an excitatory synapse marker protein, but not toward vesicular GABA transporter (VGAT), an inhibitory

synapse marker protein (Fig. 2-4a,b). As expected, PDK could induce presynaptic differentiation when they met only with the fully developed cells (DIV14), showing slightly weaker hemisynapses than NL-1R as shown in (Fig. 2-3c and Fig. 2-4c). When we elongated the incubation up to 8 d, however, the majority of the synaptic boutons generated by the PDK beads diminished while the ones induced by the NL1-R beads increased (Fig. 2-4d). When the beads were seeded on DIV7, only NL1-R exerted synaptogenic activity upon incubation for 8 d (Fig. 2-4e-h), similar to the result for NL1-R seeded on DIV14 (see Fig. 2-4c). The polybasic molecules such as PDK, if applied to developed neurons, can satisfy the eager for the synaptogenesis of outgrowing axons by allowing hemisynapse formation. It seems, however, that the factors sustaining hemisynapses become accustomed to the PDK molecules and eventually lose their synaptogenic potential upon extended period of coincubation. In comparison, the NL1-R artificial dendrites not only induced excitatory hemisynapses with neurons at any developmental stages but also strengthened and maintained the excitatory specificity of the synapses as long as live neurons are provided.

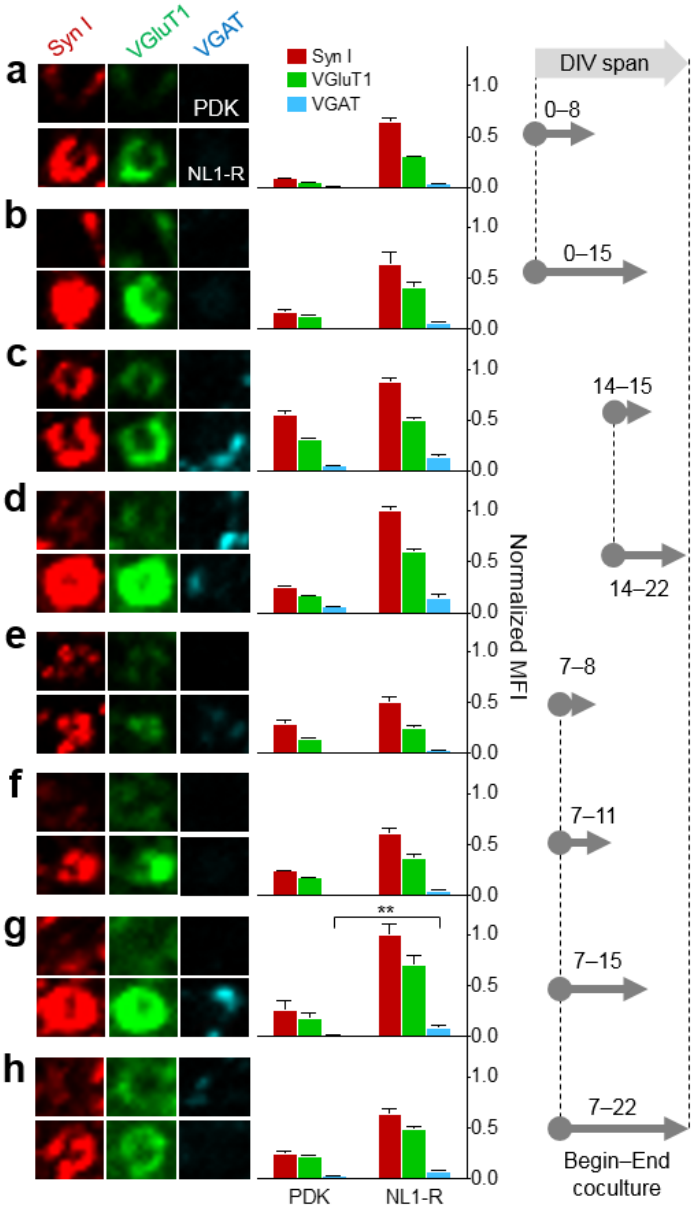


**Fig 2-4** NL1-R induces the formation of glutamatergic presynaptic boutons regardless of the developmental stages of cultured neurons and the incubation period. (a-h) ICC imaged for PDK-induced hemisynapses are aligned on upper lines. The cells were doubly stained either by anti-synapsin I (Syn I, red), VGluT1 (green), and VGAT (cyan). The PDK and NL1-R beads were seeded on DIV0 and incubated for 8 d (a) and 15 d (b). The beads seeded on DIV14 were incubated for 1 d (c) and 8 d (d). When seeded on DIV7, the incubation was continued for 1 d (e), 4 d (f), 3 d (g), and 15 d (h). **p<0.01; others p<0.001 between the same marker proteins.

### 2.3.4 Inhibitory presynaptic differentiation induced by NL2-R and SL3-R

We next applied the NL2-R- and SL3-R-coated inhibitory artificial dendrites on neuron cultures in various developmental stages to compare the timing of the instruction of inhibitory hemisynapses. When we added NL2-R or SL3-R beads to immature neuronal cells (DIV0 and 7), we could observe only excitatory presynaptic differentiation regardless of the coculture duration (Fig. 2-5a-d). The inhibitory synaptic specificity appeared when the coculture started on DIV9 and was fully restored on DIV14 (Fig. 2-5e-g). Thus, it was the timing of the encounter with artificial dendrites that determined the inverted synaptic specificity of growing neurons.

In the developing hippocampal neurons, GABAergic synapses are formed before glutamatergic synapses [37]. In the dissociated hippocampal neurons, however, the formation of glutamatergic synapses typically precedes one of the GABAergic synapses [37-38], where the mismatched synapses form frequently. This mismatch diminishes as neurons mature, probably promoted by the regulated expression of type-specific synaptic CAMs or by increased transmitter activity between matched synaptic machineries [37] including a signaling for proteolytic cleavage of synaptic adhesion proteins for sculpting of the mismatched synapses [39].

By contrast, our abiotic artificial dendrites are immune to

neurotransmitter signals and proteolytic cleavage, not allowing correction of initially formed mismatched specificity. It is possible that the NL1-R-induced glutamatergic hemisynapses found in the immature hippocampal neurons (see Fig. 2-4) originate in part from a simple mismatch independent of the type-specific synaptic CAMs. Thus, in classical culture of hippocampal neurons, the synaptic specificity defined by the synaptic vesicle proteins is determined not by the synaptic CAMs but by the degree of neuronal development.

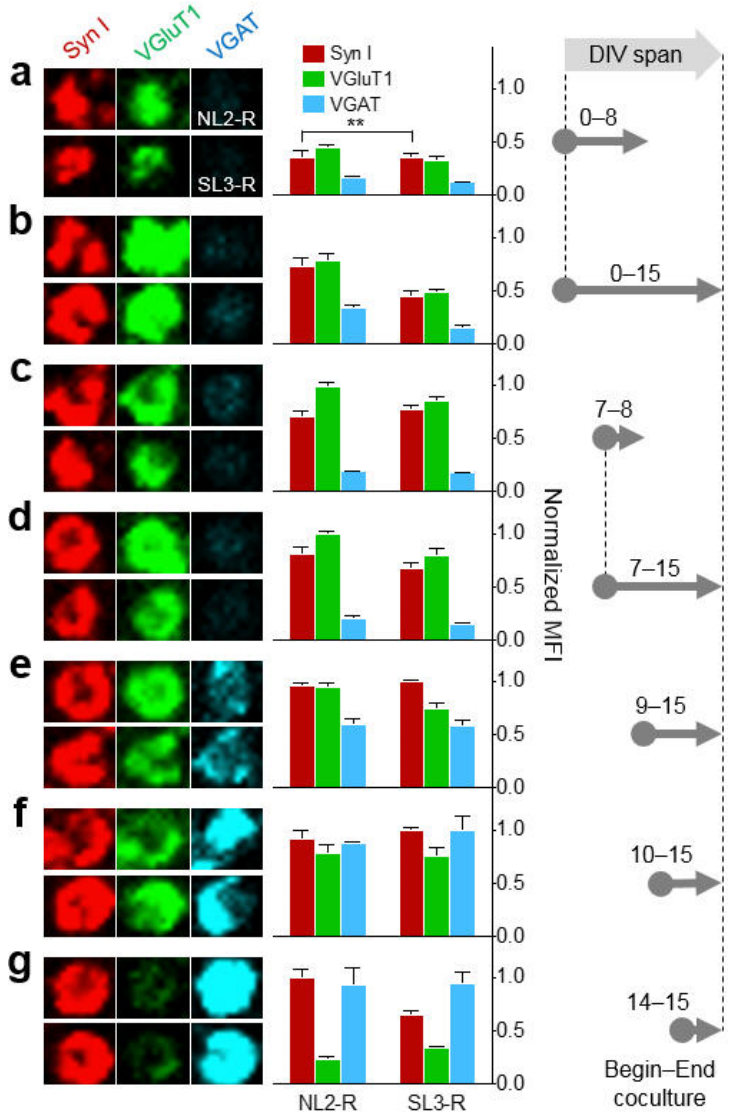


**Fig 2-5** NL2-R and SL3-R induce the formation of inhibitory hemisynapses only with mature neurons. The NL2-R and SL3-R beads were seeded and analysed for the synaptogenesis as in the case of NL1-R. (a-g) ICC images for NL2-R-induced hemisynapses are aligned on upper lines. (a-d) Only excitatory presynaptic differentiations appeared during the early neuronal development stages, which lasted until DIV15. Correctly matched synapses began to appear on DIV9 when the glutamatergic specificity is still dominant (e). The fully inhibitory hemisynapses could be formed only when the artificial dendritic beads are in contact with mature neurons (DIV14) (g). **p<0.01; others, p<0.001 between the same marker proteins of NL2-R and SL3-R.

### 2.3.5 Type-specific synaptic networks with artificial dendrites in the axonal compartmentalization

In the brain, neurons manifest a polarized subcellular structure and complex geometry through which the formation of synapses by the synaptic CAMs is chronologically and geometrically controlled. In order to address the functional importance of the subcellular synaptic specificity, we reconstituted spatial compartmentalization using microfluidic culture chamber that enables isolation of axons from somata in an analogous fashion to the patterned hippocampal neural networks [20,26-27]. The directional growth of neurons provides a homogeneous population of axons with which the postsynaptic CAM-covered solid substrates can form hemisynapses without intervening endogenous dendrito- and somato-axonic synapses (Fig. 2-6a-c).

About one week after seeding the neuronal cells in the left somal side of the chamber, axons escaped the microchannels to reach the right compartment of the chamber and covered about two-thirds of the field on DIV14. After brief verification of synaptogenic activity of NL1-R beads (Fig.2-7), we applied artificial dendrites displaying NL1-R, NL2-R, and SL3-R to the axonal compartments and compared the developmental pattern of the synaptic specificity. As expected, in the axonal compartment of adult neurons the artificial dendrites exerted correctly matched synaptic specificity, similar to the results obtained from random-cultured mature neurons (Fig. 2-5d; also see Fig. 2-3 and 2-4). Surprisingly, when we seeded the

synaptic CAM beads on DIV7 and incubated for 8 d, there was no inversion of synaptic specificity caused by inhibitory NL2-R and SL3-R beads (Fig. 2-5e), showing similar patterns of synaptic puncta between the beads near and far from the microchannels (Fig. 2-8). Thus, in order to induce correctly matched hemisynapses, the artificial dendrites appear to require isolated axonal components of cultured neurons.

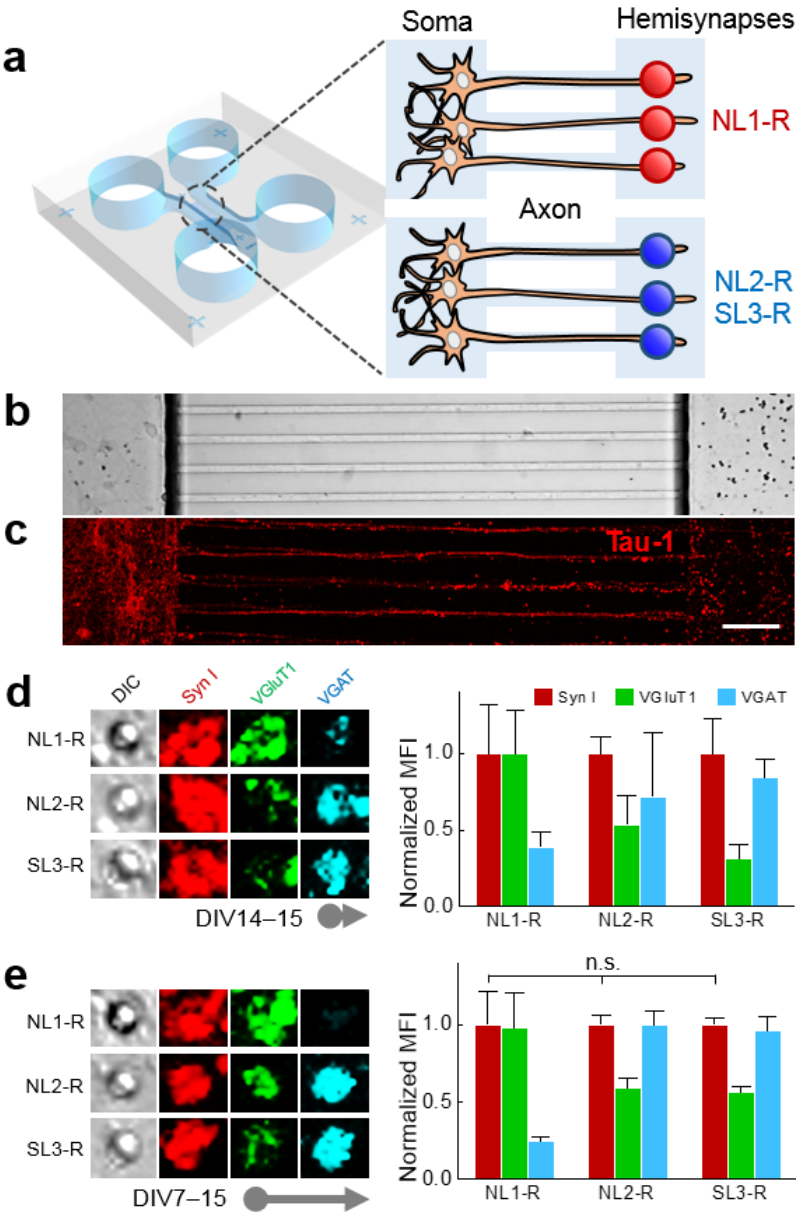


**Fig 2-6** Axons are compartmentalized to mimic patterned neural networks found in hippocampus. (a) Schematics showing isolated axons in contact with excitatory (NL1-R) and inhibitory (NL2-R and SL3-R) artificial dendrites. Light image (b) and Tau-1 staining (c) shows aligned axon bundles with seeded neurons on the left and the artificial dendrites on the right. Scale bar = 20 $\mu$m. (d) The neuronal cells and the NL1-R beads were incubated for 1 d form DIV14 (d) and for 8 d form DIV7 (e) followed by the ICC analysis. n.s., not significant; others, $p<0.001$ between the same marker proteins of NL1-R, NL2-R, and SL3-R.

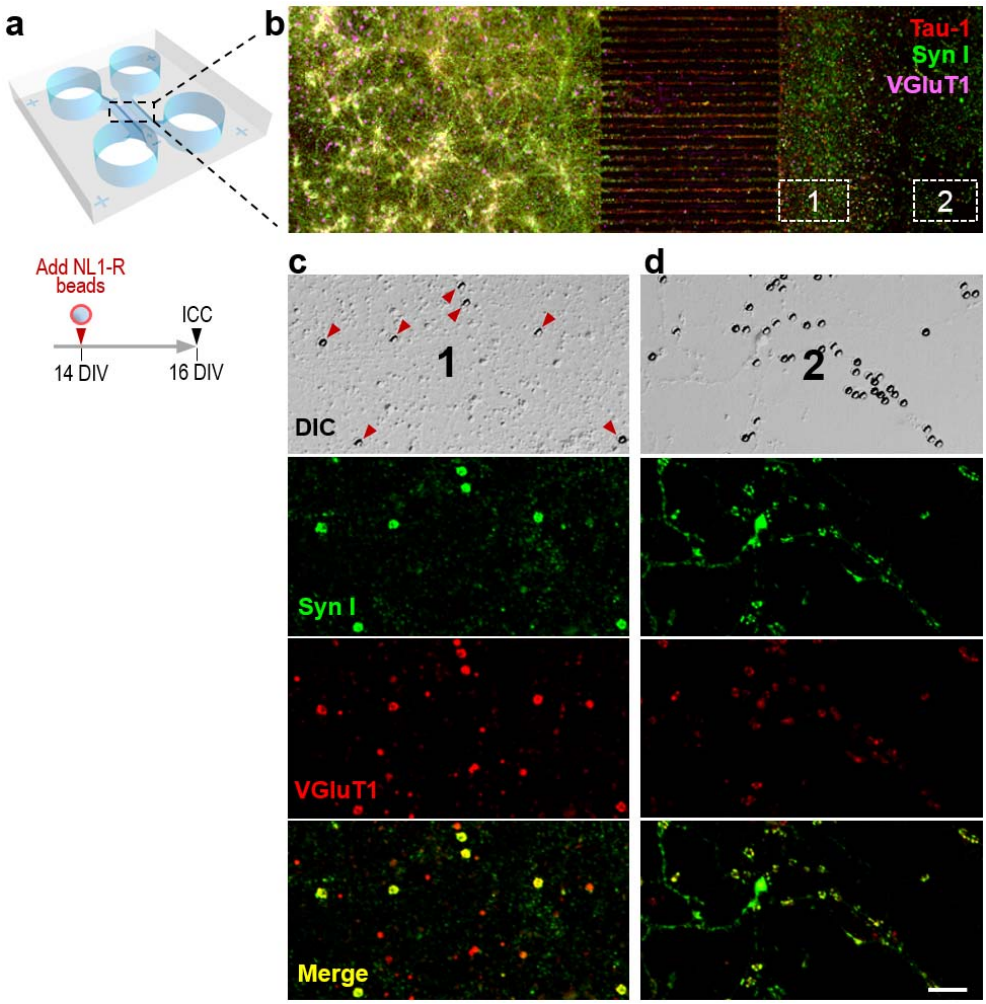


Fig 2-7 Axons isolated by compartmentalized culture chamber can elicit glutamatergic presynaptic differentiation. (a) On the axonal compartment the NL1-R displaying artificial dendritic beads were seeded on DIV14 and incubated for 2 d. (b) Immunoreactivity of Tau-1, Syn I, and VGlut1. Tau-1 is an axonal marker protein. (c) The artificial dendrites near the microchannel exits exhibit stronger fluorescent puncta (red arrowheads), due to the longer co-culture period, than the ones on outgrowing axonal terminals (d). Scale bar = 15 $\mu$m.

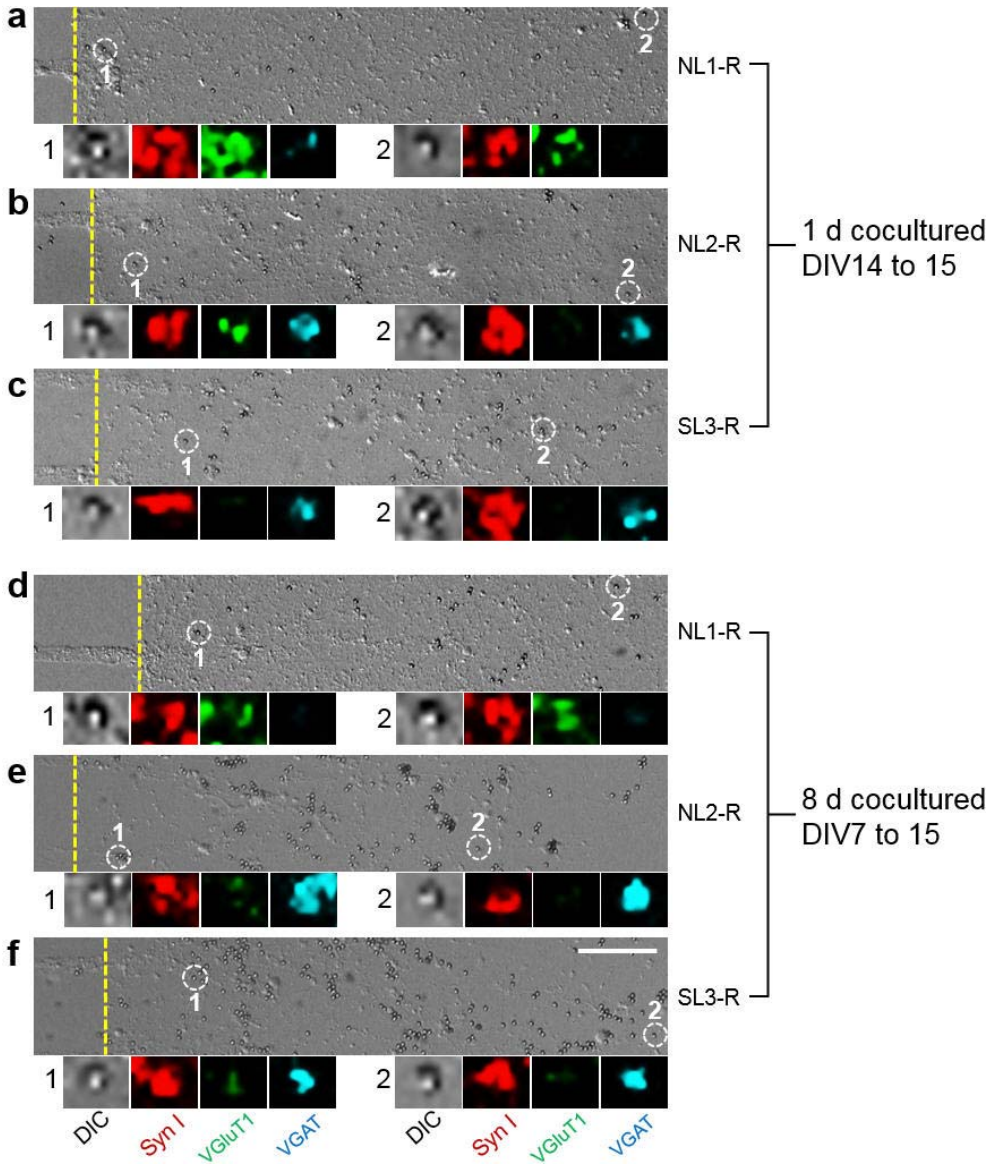


**Fig. 2-8** Synaptic specificity induced by the artificial dendrites showed little difference at near (a-c) and far from (d-f) the microchannels regardless of the seed timing of the dendritic beads. The end of the microchannels is indicated by yellow broken lines. Scale bar = 50 $\mu$m.

### 2.3.6 Spatiotemporal measurements of glutamate secreted by neurons using the engineered glutamate sensing protein, iESF

We designed a modified version of the intensity-based glutamate (Glu) sensing fluorescent protein, iGluSnFR, carrying N-terminal hexa-histidine tag (6 × His) and biotin acceptor peptide (AP or AviTag) (Fig. 2-9). The AP consists of 15 amino acids (GLNDIFEAQKIEWHE) in which Lys residue is *in vivo* biotinylated by endogenous bacterial biotin holoenzyme synthetase (BirA) [40], enabling easy conjugation of the protein with any type of SAV coated surfaces (Fig. 2-9). The engineered protein iGluSnFR, dubbed iESF, was overexpressed in *E. coli* BL21 (DE3) and purified by Ni-NTA affinity chromatography, showing a single 66 kDa band on SDSPAGE analysis (Fig. 2-10a). The in vivo biotinylation of the purified iESF was directly assessed using Dynabeads. The iESF loaded microbeads showed saturation in the signal-to-noise ratio (SNR), expressed as $\Delta F/F = (F - F_0)/F_0$, when 6 $\mu$g of the proteins were incubated with $6 \times 10^5$ beads in the presence of 1 mM Glu, indicating that the protein is *in vivo* biotinylated in the active form. The SNR of the microbeads fully loaded with iESF increased according to the Glu input (Fig. 2-10b and c).

We harnessed the microsensors in a single bead-based assay of Glu spillover by stimulated neuronal cells with multiplexed spatial resolution. Hippocampal neurons were cultured for 15 days *in vitro*

(DIV) before an extensive wash with DPBS containing $CaCl_2$ to remove residual Glu in the culture medium (Fig. 2-11a). We then spread the iESF microsensors on neurons and incubated for 10 min before stimulation by potassium shock (200 mM final concentration in DPBS). When we analyzed the captured images, SNR of the microsensors near the complex neuronal connections peaked within 2 s (Fig. 2-11b, left panels and Fig. 2-11c filled circles), whereas near the isolated neurites did not (Fig. 2-11b, right panels and Fig. 2-10c empty circles). Thus, the iESF microsensors were able to localize neuronal network regions where Glu neurotransmitters are actively secreted upon stimulation.

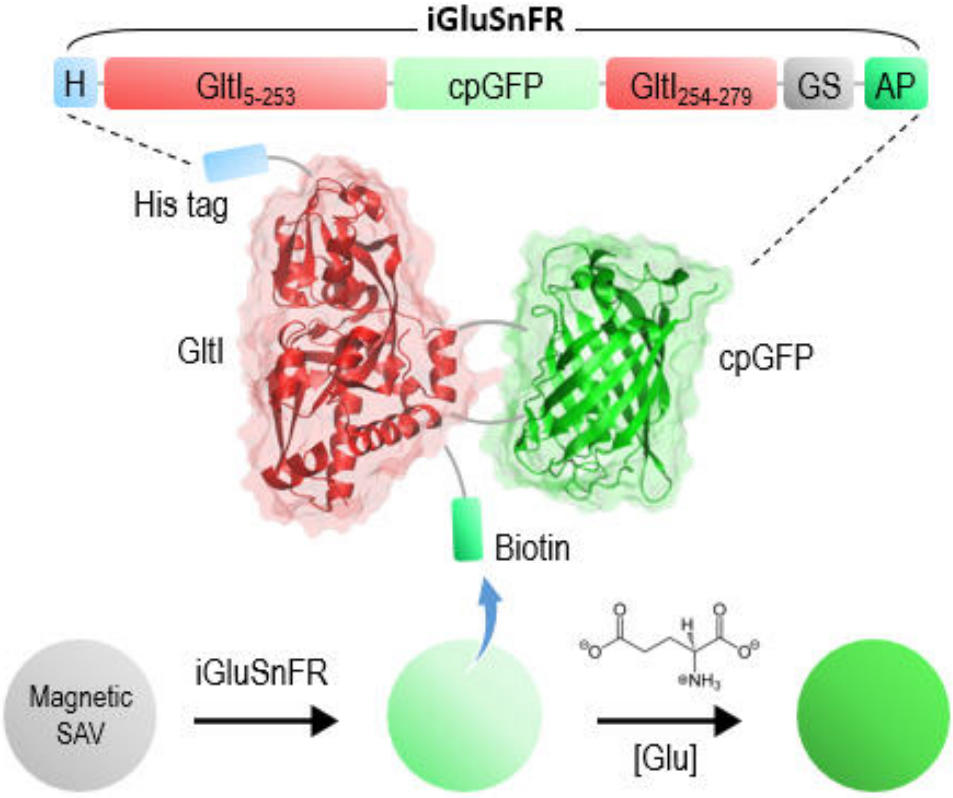


**Fig. 2-9** Genetically engineered iGluSnFR (iESF) for *in vivo* biotinylation can be immobilized on streptavidin (SAV)-coated microbeads with ease, which is used for the detection of glutamate (Glu) secreted by neurons.

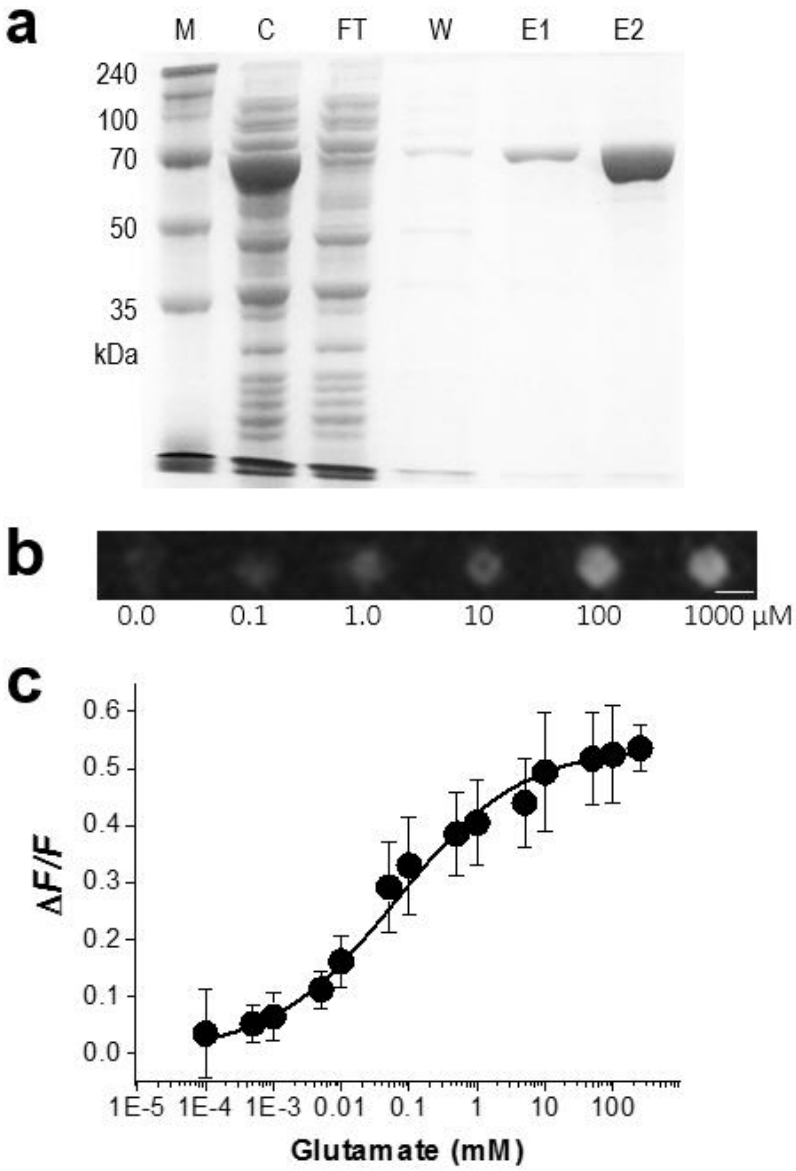


Fig. 2-10 Glutamate (Glu) dose-response of iESF microbeads. (a) Affinity column purification of the *in vivo* biotinylated iESF. M, protein markers; C, cell lysate; FT, flow through; W, wash; E, elution. (b) Fluorescence images of the iESF-immobilized microbeads upon Glu input (0 - 1000 $\mu$M). (c) Titration of the iESF microsensor ($n$ = 10 per point) with Glu using fluorescence microscopy.

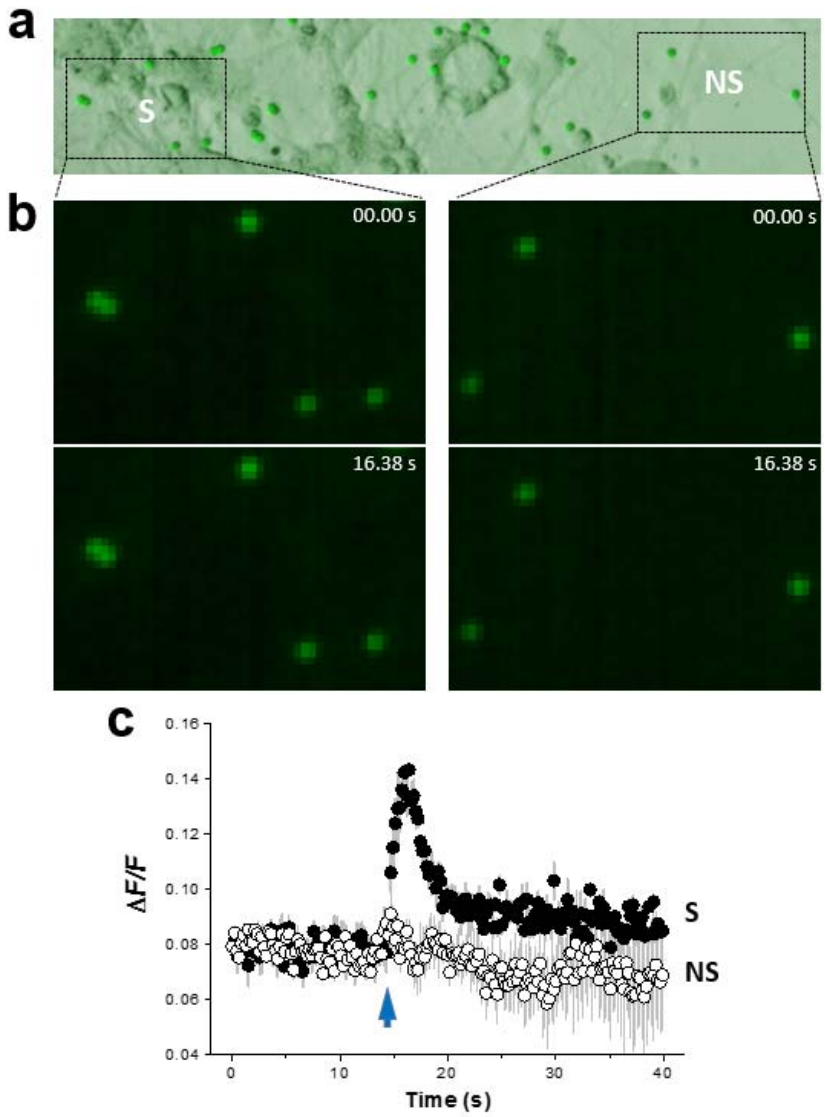


**Fig. 2-11** (a) Coincubation of the iESF microsensors and hippocampal neurons on DIV15. The SNR ($\Delta F/F$) of the iESF microsensors spread near the intertwined neurites (region S) peaked at 16.38 s after the neuronal stimulation (b, left panels and c, filled circled), whereas the sensors near the isolated neurites (region NS) showed no changes in SNR (b, right panels and c, empty circles).

### 2.3.7 Glutamatergically active-presynaptic boutons induced by NL1-R

Having established the polarized artificial synaptic interfaces, we wanted to ensure the synaptic functionality of the hemisynapses to genuinely mimic the directional flow of neuronal information via neurotransmitters. We thus used the engineered iESF [40] to directly measure the rapid glutamate transients. As a result of the previous study, the engineered iESF shares C-terminal tagging module with our synaptic CAM ectodomains and has the sensitivity enough for our experiments. We placed the NL1-R beads in the axonal side of the culture chamber on 14 DIV, allowing two days of hemisynapse formation before spreading the freshly prepared iESF beads (Fig. 2-12a,b). Upon potassium shock in the somal side of the chamber, we could observe an increase in green fluorescence of iESF near NL1-R beads in comparison to SAV beads without NL1-R, indicating that the hemisynapses possess type-specific neurotransmitter activity (Fig. 2-12c).

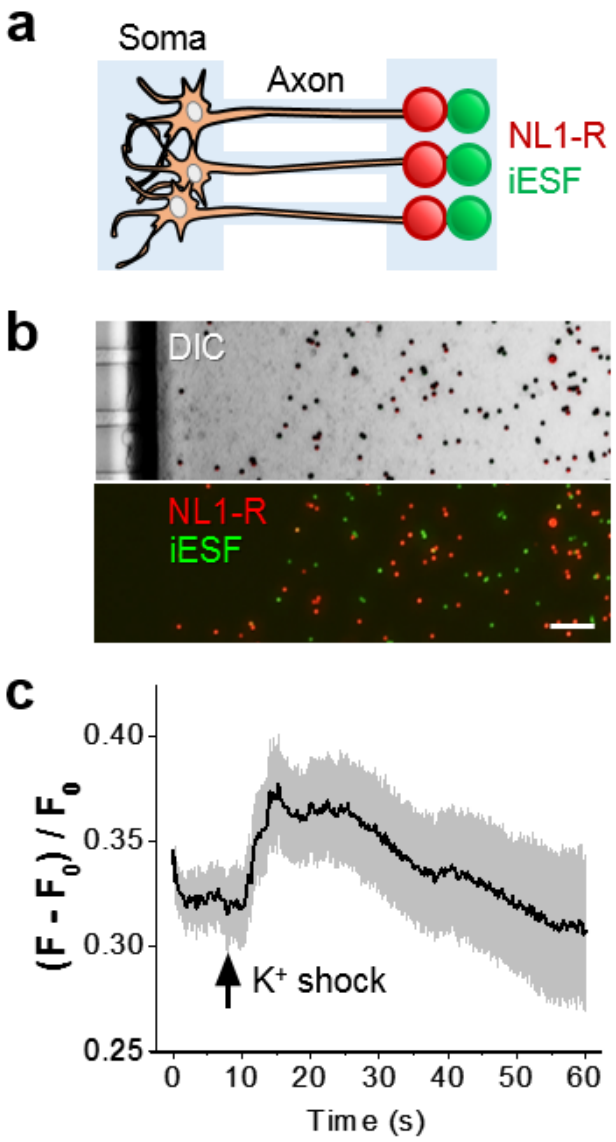


**Fig. 2-12** Excitatory hemisynapses release glutamate neurotransmitters. (a) Schematics of the measurement of glutamate spillover using engineered glutamate sensor iESF. (b) NL1-R artificial dendrites were added to the axonal compartment of DIV14 cells. After incubation for 2 d, the iESF beads were spread to the same side. Scale bar = 10 $\mu$m. (c) The neurons were stimulated by potassium shock on the somal compartment. When compared with bare SVA beads, the iESF beads near the artificial dendrites exhibited enhanced fluorescence due to the glutamate spillover.

## 2.4 Conclusion

Abiotic solid substrata displaying engineered ectodomains of postsynaptic CAMs can serve as artificial dendrites, inducing the formation of durable excitatory and inhibitory hemisynapses with spatiotemporal regulation. The ectodomains of NL1, NL2, and Slitrk3 allow C-terminal tagging for optical tracking and surface immobilization that dispenses with lipid bilayers for its synaptogenic activity. The modular C-terminal tags may change ectodomains of virtually any pre- and postsynaptic CAMs that have functional extracellular domains. Notably, the artificial dendrites could instruct the formation of inhibitory hemisynapses with dissociated culture of well-developed neurons and with an isolated axonal component of micropatterned neurons even in their early developing stages. Once determined, either the matched or mismatched synaptic specificity of hemisynapses remained unchanged during the extended neuronal development. Such robust hemisynapses should bode well for a fundamental study on information process of neural networks in the brain and novel type of synapse-based biointerfaces where signals are transduced via synaptic boutons with defined synaptic specificity and spatial geometry.

## 2.5 References


[1] M. B. Dalva, A. C. McClelland and M. S. Kayser, *Nat. Rev. Neurosci.*, 2007, *8*, 206.

[2] H. Hu, J. Gan, and P. Jonas, *Science*, 2014, *345*, 529.

[3] R. A. Normann, *Nat. Clin. Pract. Neuro.*, 2007, *3*, 444.

[4] G. Orive, E. Anitua, J. L. Pedraz, and D. F. Emerich, *Nat. Rev. Neurosci.*, 2009, *10*, 682.

[5] C. Dean, F. G. Scholl, J. Choih, S. DeMaria, J. Berger, E. Isacoff and P. Scheiffele, *Nat. Neurosci.*, 2003, *6*, 708.

[6] M. M. Baksh, C. Dean, S. Pautot, S. DeMaria, E. Isacoff and J. T. Groves, *Langmuir*, 2005, *21*, 10693.

[7] K. Czondor, M. Garcia, A. Argento, A. Constals, C. Breillat, B. Tessier and O. Thoumine, *Nat. Commun.*. 2013, *4*, 2252.

[8] G. Gopalakrishnan, P. Thostrup, I. Rouiller, A. L. Lucido, W. Belkaid, D. R. Colman and R. B. Lennox, *ACS Chem. Neurosci.*, 2010, *1*, 86.

[9] A. L. Lucido, G. Gopalakrishnan, P. T. Yam, D. R. Colman and R. B. Lennox, *ACS Chem. Neurosci*,. 2010, *1*, 535.

[10] A. L. Lucido, F. S. Sanchez, P. Thostrup, A. V. Kwiatkowski, S. L.-Ortiz, G. Gopalakrishnan, D. Liazoghli, W. Belkaid, R. B. Lennox, P. Grutter, C. C. Garner and D. R. Colman, *J. Neurosci.*, 2009, *29*, 12449.

[11] T. C. Sudhof, *Nature*, 2008, 455, 903.

[12] B. Chih, H. Engelman and P. Scheiffele, *Science*, 2005, *307*, 1324.

[13] B. Chih, L. Gollan and P. Scheiffele, *Neuron*, 2006, *51*, 171.

[14] J. Y. Song, K. Ichtchenko, T. C. Sudhof and N. Brose, *Proc. Natl. Acad. Sci.*, 1999, *96*, 1100.

[15] G. Giannone, M. Mondin, D. G.−Bosch, B. Tessier, E. S.−Michel, K. Czondo r, M. Sainlos, D. Choquet and O. Thoumine, *Cell Rep.*, 2013, *3*, 1996.

[16] M. Missler, T. C. Sudhof and T. Biederer, *Perspect. Biol.*, 2012, *4*, a005694.

[17] H. Takahashi, K. Katayama, K. Sohya, H. Miyamoto, T. Prasad, Y. Matsumoto, M. Ota, H. Yasuda, T. Tsumoto, J. Aruga and A. M. Craig, *Nat. Neurosci.*, 2012, *15*, 389.

[18] Y. S. Yima, Y. Kwonb, J. Nam, H. I. Yoon, K. Lee, D. G. Kim, E. Kim, C. H. Kim and J. Ko, *Proc. Natl. Acad. Sci.*, 2013, 110, 4057.

[19] A. Takeuchi, S. Nakafutami, H. Tani, M. Mori, Y. Takayama, H. Moriguchi, K. Kotani, K. Miwa, J. Lee, M. Noshirod and Y. Jimbo, *Lab Chip*, 2011, *11*, 2268.

[20] A. M. Taylor, D. C. Dieterich, H. T. Ito, S. A. Kim and E. M. Schuman, *Neuron*, 2010, *66*, 57.

[21] J.−M. Peyrin, B. Deleglise, L. Saias, M. Vignes, P. Gougis, S. Magnifico, S. Betuing, M. Pietri, J. Caboche, P. Vanhoutte, J.−L. Viovy and B. Brugg, *Lab Chip*, 2011, *11*, 3663.

[22] S. Pautot, H. Lee, E. Y. Isacoff and J. T. Groves, *Nat. Chem. Biol.*, 2005, *1*, 283.

[23] P. Shi, M. A. Scott, B. Ghosh, D. Wan, Z. Wissner-Gross, R. Mazitschek, S. J. Haggarty and M. F. Yanik, *Nat. Commun.*, 2011, *2*, 510.

[24] Y. H. Hsu, H. I. Wu, W. S. Cheng, H. W. Chung, T. Y. Wu, Y. C. Chang, *Anal. Biochem.*, 2012, *427*, 1.

[25] J. Woo, S.-K. Kwon, S. Choi, S. Kim, J.-R. Lee, A. W. Dunah, M. Sheng and E. Kim, *Nat. Neurosci.*, 2009, *12*, 428.

[26] A. M. Taylor, M. Blurton-Jones, S. W. Rhee, D. H. Cribbs, C. W. Cotman and N. L. Jeon, *Nat. Methods*, 2005, *2*, 599.

[27] J. W. Park, B. Vahidi, A. M. Taylor, S. W. Rhee and N. L. Jeon, *Nat. Protoc.*, 2006, *1*, 2128.

[28] J. S. Marvin, B. G. Borghuis, L. Tian, J. Cichon, M. T. Harnett, J. Akerboom, A. Gordus, S. L. Renninger, T.-W. Chen, C. I. Bargmann, M. B. Orger, E. R. Schreiter, J. B. Demb, W.-B. Gan, S. A. Hires and L. L. Looger, *Nat. Methods*, 2013, *10*, 162.

[29] S. Y. Lee, E. J. Kim, J. S. Kim, I. Hwang and T. D. Chung, *Chem. Commun.*, 2016, *52*, 11854.

[30] D. Comoletti, R. Flynn, L. L. Jennings A. Chubykin, T. Matsumura, H. Hasegawa, T. C. Sudhof and P. Taylor, *J. Biol. Chem.*, 2003, *278*, 50497.

[31] D. Arac , A. A. Boucard, E. Ozkan, P. Strop, E. Newell, T. C. Sudhof and A. T. Brunger, *Neuron*, 2007, *56*, 992.

[32] X. Chen, H. Liu, A. H. R. Shim, P. J. Focia and X. He, *Nat. Struct. Mol. Biol.*, 2008, *15*, 50.

[33] M. Howarth and A. Y. Ting, *Nat. Protoc.*, 2008, *3*, 534.

[34] A. Rao, E. M. Cha and A. M. Craig, *J. Neurosci.*, 2000, *20*, 8344.

[35] I. Brunig, A. Suter, I. Knuesel, B. Luscher and J. M. Fritschy, *J. Neurosci.*, 2002, *22*, 4805.

[36] S. Hennou, I. Khalilov, D. Diabira, Y. Ben-Ari and H. Gozlan, *Eur. J. Neurosci.*, 2002, *16*, 197.

[37] Y. Ben-Ari, J. L. Gaiarsa, R. Tyzio and R. Khazipov, *Physiol. Rev.*, 2007, *87*, 1215.

[38 J. W. Um, K. H. Kim, B. S. Park, Y. Choi, D. Kim, C. Y. Kim, S. J. Kim, M. Kim, J. S. Ko, S.-G. Lee, G. Choii, J. Nam, W. D. Heo, E. Kim, J.-O. Lee, J. Ko and H. M. Kim, *Nat. Commun.*, 2014, *5*, 5423.

[39] M. Källberg, H. Wang, S. Wang, J. Peng, Z. Wang, H. Lu, J. Xu, *Nat. Protoc.*, 2012, *7*, 1511.

[40] J. S. Marvin, B. G. Borghuis, L. Tian, J. Cichon, M. T. Harnett, J. Akerboom, A. Gordus, S. L. Renninger, T.-W. Chen, C. I. Bargmann, M. B. Orger, E. R. Schreiter, J. B. Demb, W.-B. Gan, S. A. Hires and L. L. Looger, *Nat. Methods*, 2013, *10*, 162.

# Part 2.

## Electrochemical Study at Artificial Synapse Induced between Surface Modified Electrode and Neuron

# 3. Electrochemical Study at Artificial Synapse Induced between Surface Modified Electrode and Neuron

## 3.1 Introduction

In the field of neural interface, it has achieved remarkable outcomes in helping the neurological disorders, such as Parkinson's disease, Lou Gehrig's disease, and spinal cord injury, by controlling the neural signals though a direct connection between the brain and the electronics. This is because many technologies related to neuroscience have been consistently investigated and developed together in various other fields. Studies in terms of neuro-engineering have been focused on the main purpose of understanding neural networks as well as applying neuro-therapeutics or prosthetics by recording nerve signals of the brain using implantable or non-implantable electrodes; at this time, the target signals include electroencephalograms (EEGs), electrocorticograms (ECoGs), local field potentials (LFPs), or spikes. And in the flow of academic research, numerous types of neural electrodes for sensitive sensing of neural signals, such as an action potentials (APs) or neurotransmitters, have been reported by developing new materials or efficient structures of the electrodes [1-5].

The conventionally signaling processing of these existing technologies relies solely on physical and passive contacts between non-biological electronic devices and neurobiological components (tissue or cells). However, in the actual brain system, there is close communication between neurons via chemical synapse, in which transmission of neural information occur. The neurotransmission through a narrow synaptic cleft is accomplished by converting action potentials (APs) of electrical signals into neurotransmitters that are chemical messengers [6-7]. The neurotransmitter depending on whether it is an excitatory or inhibitory synapse is the key factor that determines whether or not to transmit the presynaptic information to the postsynaptic neurons. These synaptic systems actually connect neural networks in the brain and are involved in not only normal functioning of the nervous system but also regulation of cognitive functions such as learning, memory, thinking, and emotion. Therefore, in order to thoroughly examine the working mechanism and function of the complicated neural networks, it is necessary to understand the chemical synaptic transmission and distinguish significant synaptic signals, such as excitatory or inhibitory signals, from complex neural signals.

Several studies focused on the synapse have been trying to understand of synaptic behaviors, and have been reported using electrochemical measurement method that is one of useful techniques that have a high spatial and temporal resolution applicable to neuroscience. However, they have merely strived to monitor APs or

electroactive neurotransmitters by electrochemical amperometric measurements or potentiometric recordings using ultramicroelectrode or nanoelectrode nearest to synapse or inside the synaptic cleft [8-12]. As a new approaching strategy unlike with such the existing system mentioned above, we propose an artificial synaptic interface to be active neural interface based on synapse. By constructing type-specific and durable artificial synapse on the non-biological electrode, it can be possible to directly detect meaningful synaptic signals and to bilaterally communicate to neuron with regulating spatiotemporal feedback. In addition, if the artificial synapse interface was regarded as a bio-electric hybrid nanogap, the mechanism of electrical and chemical signals across the synapse cleft can be electrochemically investigated and information processing via artificial synapse can be sophisticatedly realized.

Recently, we have reconstituted artificial neuronal hemisynapses using engineered postsynaptic cell adhesion molecules (CAMs) immobilized on polymer microbeads [13]. By tagging the ectodomains of postsynaptic CAMs, such as neuroligin 1 (NL1), neuroligin 2 (NL2), and Slitk3 (SL3), with biotin and red fluorescent protein (RFP), they could be efficiently immobilized on the surface of micro-substrates and selectively induced robust and type-specific hemisynapses. Here, based on the previous results, we report for replacing the postsynaptic neurons that receive the signals in neural networks with the modified hybrid microelectrodes in order to construct the artificial synaptic interface (see Fig. 3-1). We chose

a commercialized microelectrode array (MEA) that has been widely applied in the field of neuroscience research; the electrodes of the MEA are made of titanium nitride (TiN). And we performed the surface modifications, which is an electrochemical plating of gold (Au) that is a good candidate for inert and biocompatible metal. The Au plated TiN electrodes have rough surface similar to porous structure, thereby the quality of electrode can be improved with large surface area, low electrode impedance and enhanced signal-to-noise ratio (SNR), and the surface of electrode can be easily functionalized with chemicals or biomolecules such as self-assembled monolayer (SAM) formation reagent, streptavidin, and the biotinylated postsynaptic CAM NL1. Consequently, we successfully fabricated the modified microelectrode substituting the postsynaptic neuron portion, and then the artificial hemisynapses induced to primary hippocampal neurons contacted with the postsynaptic electrodes were stably maintained the property of excitatory glutamatergic synapse.

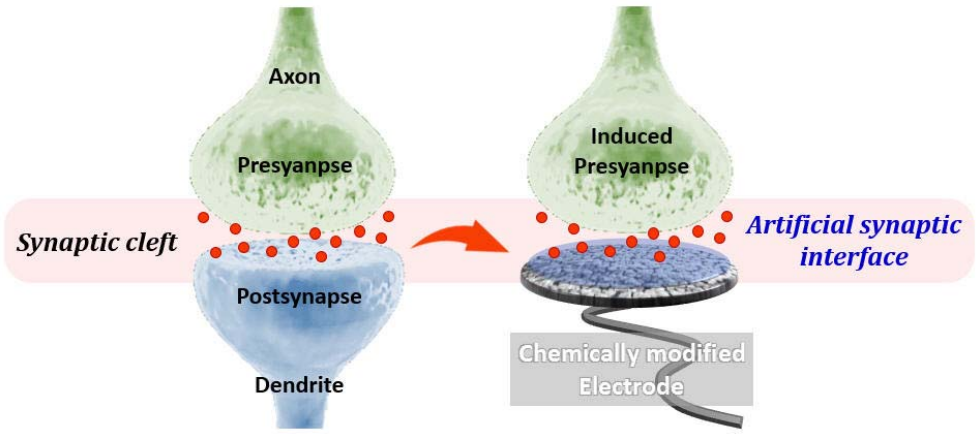


Fig. 3-1 Scheme for construction of the artificial synaptic interfaces by replacing the postsynaptic neurons receiving the neural signals in the brain networks with the chemically surface-modified postsynaptic electrodes.

## 3.2 Experimental Methods

### 3.2.1 Materials and reagents

Pt wire (500 $\mu$m, Aldrich) for the counter electrode and Ag/AgCl (in saturated KCl, CH Instruments Inc.) or $Hg/Hg_2SO_4$ (in saturated $K_2SO_4$, CH Instruments Inc.) for the reference electrode were used. Sodium tetrachloroaurate (III) ($NaAuCl_4$, 298174) and hexaammineruthenium (III) chloride ($Ru(NH_3)_6Cl_3$, 262005) were purchased from Aldrich. Sodium perchlorate ($NaClO_4$, 310514) and sodium chloride (NaCl, S7653) were from Sigma-Aldrich. Phosphate buffered saline (PBS) was prepared by mixing 0.1 M sodium hydrogen phosphate ($Na_2HPO_4$, Sigma-Aldrich S7907) and 0.1 M sodium dihydrogen phosphate ($NaH_2PO_4$, Sigma-Aldrich S8282) containing 0.15 M NaCl. Potassium hexacyanoferrate (III) ($K_3Fe(CN)_6$, P8131), poly-D-lysine (PDK, Mw 70,000-150,000, P0899), laminin (L2020), streptavidin (85878) and triton X-100 (X100) were from Sigma. Sulfuric acid ($H_2SO_4$, 7683), potassium nitrate ($KNO_3$, 6603), and ethanol (EtOH, 4022) were purchased from Daejung. Biotin-SAM formation reagent (b564) was from Dojindo. Dulbecco's Phosphate Buffered Saline (DPBS, LB001-02) was from Welgene. Paraformaldehyde (P2031) was purchased from Biosesang and normal donkey serum (017-000-121) was from Jackson ImmunoResearch Inc. Mouse synapsin I monoclonal antibody (106 001) from Synaptic Systems and guinea pig VGluT1 (vesicular

glutamate transporter1) polyclonal antibody (AB5905) from Millipore were purchased, respectively. For secondary antibodies, we used anti-mouse and anti-guinea pig conjugated with Alexa Fluor 488 and 633 (Invitrogen A11029 and A21105, respectively). All aqueous solutions in this experiment were prepared with ultrapure deionized water (DI water) produced by NANOpure (Barn-stead).

### 3.2.2 MEA preparation

MEAs with titanium nitride (TiN) electrodes (in size of 30 $\mu$m with inter-electrode distance of 200 $\mu$m) and indium tin oxide (ITO) track-lines/contact-pads (60MEA200/30iR-ITO) were commercially obtained from Multi Channel Systems. The first step in preparing the MEA was the treatment of hydrophilic surface because the surface of new MEA was hydrophobic. MEA was rinsed with DI water, and then dried with $N_2$ blowing. After drying, the MEA was placed in the Plasma cleaner (Harrick Science Corp.) and treated with vacuum plasma for 4 min. As soon as the end of the plasma treatment, we immediately filled DI water in a well of the MEA. Next, hydrophilic surface of the MEA was coated with 1 mg/mL PDK in DPBS for overnight. Finally, the PDK coated MEA was washed with DI water more than three times. According to the following experiment, we proceeded additional washing with DPBS or electrolyte solutions.

### 3.2.3 Gold (Au) electrochemical deposition on PDK-coated MEA

We chose a potential pulse method (Multi-Potential Steps technique in CHI750A) for electrochemical deposition of gold (Au) on the PDK coated TiN-MEA. First, we found a potential range of electrochemical deposition for Au on PDK coated TiN-MEA by performing cyclic voltammetry against the Ag/AgCl reference electrode in solution of Au precursor (1 mM $NaAuCl_4$ in 0.2 M $NaClO_4$); voltammogram was recorded at 10 mV $s^{-1}$. To increase the coverage of Au nuclei and regulate the growth of Au on the surface of PDK coated TiN [14-16], we adjusted the duration and number of potential pulse at the high driving potential of electrodeposition, -0.4 V. The observation of the surface for electrodeposition of Au were carried out by confocal laser scanning microscopy (CLSM) and field emission - scanning electron microscopy (FE-SEM), and the structural section of electrochemically plated Au on the MEA was monitored using focused ion beam (FIB) and FE-SEM. The laser-reflected DIC (differential interference contrast) images were acquired by Zeiss LSM880 confocal laser scanning microscope. The section etching was accomplished using SII NanoTechnology Inc. FIB-SEM Hybrid system (SMI3050SE), and the FE-SEM images were taken with Zeiss MERLIN Compact FE-SEM at the Research Institute of Advanced Materials (RIAM) at Seoul National University.

### 3.2.4 Surface modification for fabrication of the postsynaptic electrodes

For fabrication of postsynaptic electrodes possible to induce artificial synapse with contacted neurons, we optimized a surface modification on the Au-electrochemically plated PDK-TiN MEA (Au-MEA). As shown in Fig. 3-2, the first step in modification process was to form biotinylated alkylthiolate self-assembled monolayer (SAM) on the Au-MEA so that we treated the ethanol solution containing 0.1 mM biotin-SAM formation reagent overnight at room temperature. Secondly, streptavidin (SAV) was introduced on the biotin-SAM formed Au-MEA by immersing in 0.75 mg/mL SAV solution (DPBS) for 1 h at room temperature. Previous two steps were needed to immobilize the engineered postsynaptic CAM that was a key point for inducing artificial synapses with neurons. Third, it was incubated with purified and concentrated the engineered NL1-R (biotinylated and RFP tagged neurologin-1) solution for overnight at 4 ° C. In order to improve a growth condition of neuronal cell on the MEA after the Au-electrodeposition and the surface modification for artificial postsynaptic electrode, coating step of another adhesion protein was finally added with 20 ng/mL laminin solution (DPBS) for overnight at 4 ° C. Between each step, washing was carried out with buffer DPBS more than five times.

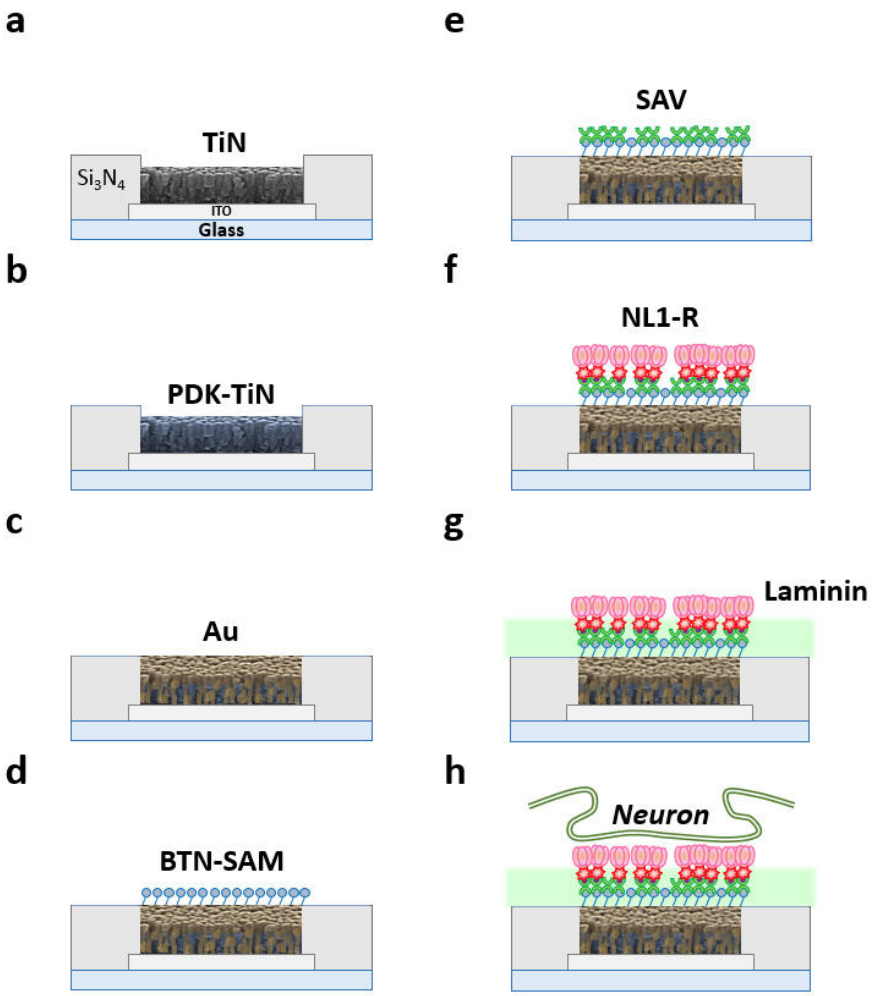


Fig. 3-2 Cross-sectional schematic illustrations from the surface modification process to neuronal cell culture for construction of the artificial synaptic interfaces. (a) Structure of a generally standard MEA consisting of titanium nitride (TiN) electrode, indium tin oxide (ITO) track-lines/contact-pads, and silicon nitride ($Si_3N_4$) insulator. (b) Coating with poly-D-lysine (PDK) on the surface of TiN MEA for neuronal cell culture. (c) Electrochemically plating gold (Au) on TiN electrode coated with PDK by the potential scan or pulse techniques. (d) Formation of biotin-tagged self-assembled monolayer (SAM) (e) Immobilization of streptavidin (SAV) (f) Immobilization of the engineered postsynaptic CAM, biotinylated neuroligin 1 (NL1-R) in key factor inducing the artificial synapses. (g) Additional coating with laminin for a more stable culture condition. (f) Finally, culture of primary hippocampal neuronal cells.

### 3.2.5 Electrochemical characterizations

All the electrochemical measurements were performed in a three-electrode electrochemical cell with Ag/AgCl reference electrode and Pt wire counter electrode at room temperature. For characterization of the modified electrode, the electrochemical experiments were carried out in PBS (pH 7.4) containing 0.1 mM $K_3Fe(CN)_6$ or 0.1 mM $Ru(NH_3)_6Cl_3$. CV (cyclic voltammetry) measurements were accomplished using a CHI750A (CH Instruments) and recorded at a potential scan rate of 50 mV s−1. EIS (electrochemical impedance spectroscopy) experiments were performed using a Model Reference 600 (Gamry Instruments), and programmed ac input with an amplitude of 10 mV in the frequency range from 0.1 Hz to 100 kHz.

### 3.2.6 Primary hippocampal neuronal cell culture

All animal studies and experimental protocols were approved by the Institutional Animal Care and Use Committee (IACUC) at Seoul National University. Primary hippocampal neurons were obtained from Sprague-Dawley rat embryos at day 18 of gestation (E18) [17]. Hippocampus dissected from E18 rat embryos were rinsed with Hank's Balanced Salt Solution (HBSS), and then treated with papain and DNase with 60 rpm for 30 min at 37 °C shaking incubation. After sequentially rinsing with solution of 10% and 5% fetal bovine serum (FBS) in HBSS, individual single cells were mechanically isolated by trituration ~10 times in 2 mL HBSS containing DNase with silanized

Pasteur pipette (the pipette tip barely polished with fire). The cell suspension was diluted to 1 × $10^5$ cells/mL with plating media containing minimum essential medium (MEM) supplemented with 0.6%wt/vol. glucose, 10 mM sodium pyruvate, 1 mg/mL FBS, 1% Penicillin-Streptomycin, and 100 $\mu$g/mL Primocin. Then, the cell-media solution plated on the MEA with seeding density of 400 cells/$mm^2$. After 3 h the cell culture media was exchanged with neurobasal medium supplemented B27 (serum free), 2 mM glutamax. Cultures were maintained under 5% $CO_2$ atmosphere in an incubator at 37 ° C. The neurobasal medium were replaced with fresh medium every 3-4 days.

### 3.2.7 Immunocytochemistry (ICC) and imaging

Neuronal cells were fixed using 4% para-formaldehyde for 25 min and rinsed once with DPBS and two times with Tris-buffered saline (TBS, pH 7.4). The cells were then incubated in blocking solution, containing 4% BSA and 0.1% Triton X-100, dissolved in TBS for 30 min, followed by incubation in primary antibodies diluted in TBS containing 0.5% BSA and 0.1% Triton X-100 for overnight at 4 ° C. The samples were then washed three times with TBS and the fluorescent secondary antibodies were applied for 1 h at room temperature in TBS containing 0.5% BSA. The samples were washed again three times with TBS and two times with filter-sterilized DDW, and stored at 4 ° C until microscopic examination. Fluorescence

images were taken with a Zeiss LSM880 confocal laser scanning microscope equipped with ZEN (black edition) software.

## 3.3 Results and Discussion

### 3.3.1 Electrochemical deposition of Au on TiN-MEA coated with PDK

For fabrication of a postsynaptic electrode, we first performed electrochemically plating of gold (Au) on a commercialized titanium nitride (TiN) microelectrode array (MEA). The commercialized TiN MEA was cleaned by plasma treatment and coated by poly-D-lysine (PDK) that is a positively charged amino acid polymer and useful in promoting cell adhesion to solid substrates. The PDK coating is generally the first step in handling to prepare cell culture on the MEA [18]. We had to do Au plating on the PDK coated MEA, so we first scanned the gold plating potentials through the cyclic voltammetry (CV). This is the first attempt to electrochemically deposit gold on a TiN electrode, but this voltammogram shape is similar to a typical CV for the electrodeposition of Au onto a two-dimensional planar carbon electrode [14-16,19]. In the electrodeposition system, the active gold precursors in the electrolyte solution are the $[AuCl_4]^-$ complex ions and the overall reaction can be expressed by $[AuCl_4]^- + 3e^- \rightarrow Au + 4Cl^-$ [16,20-21].

The cyclic voltammogram shown Fig. 3-3a illustrates the electrochemical behavior on the PDK coated TiN electrode with a diameter of 30 $\mu$m in a solution of Au precursor containing 1 mM $NaAuCl_4$ and 0.2 M $NaClO_4$. The CV was recorded at a potential scan

rate of 10 mV $s^{-1}$, commencing at +0.85 V with an initial sweep negative to −0.6 V, positive again to +1.2 V and then back to +0.85 V. On the first scan, the cathodic current by reduction of $[AuCl_4]^-$ to Au began to flow from +0.8 V, and gradually increased with applying overpotential to more cathodic potential. Inversely on the anodic−going scan, the cathodic current decreased and the anodic current peak is appeared at +1.1 V due to surface oxidation of the electrodeposited gold.

From the data obtained from the CV measurements, we performed four types of electrodeposition methods using potential scan technique and multi−potential steps technique; the four types are illustrated in Fig. 3−3b. Type [A] was potential scanning method during two segments from +0.85 V to −0.6 V at a scan rate of 10 mV $s^{-1}$ using cyclic voltammetry technique, type [B] using potential pulse method was conducted at the optimal electrodeposition potential −0.4 V with pulse duration 10 ms, and type [C], [D] were mixed potential pulse methods by varying the duration 50 ms and 10 ms on the same potential or by changing potentials from −0.4 V to 0.0 V at the same duration. Since the electrochemical deposition of gold using the potential pulse methods, such as type [B] ~ [D], was derived from the electrochemical formation of gold nanoparticles on the electrodes of carbon material [14−16], we expected that the surface of the electroplated Au on the PDK coated TiN MEA was would have been porous.

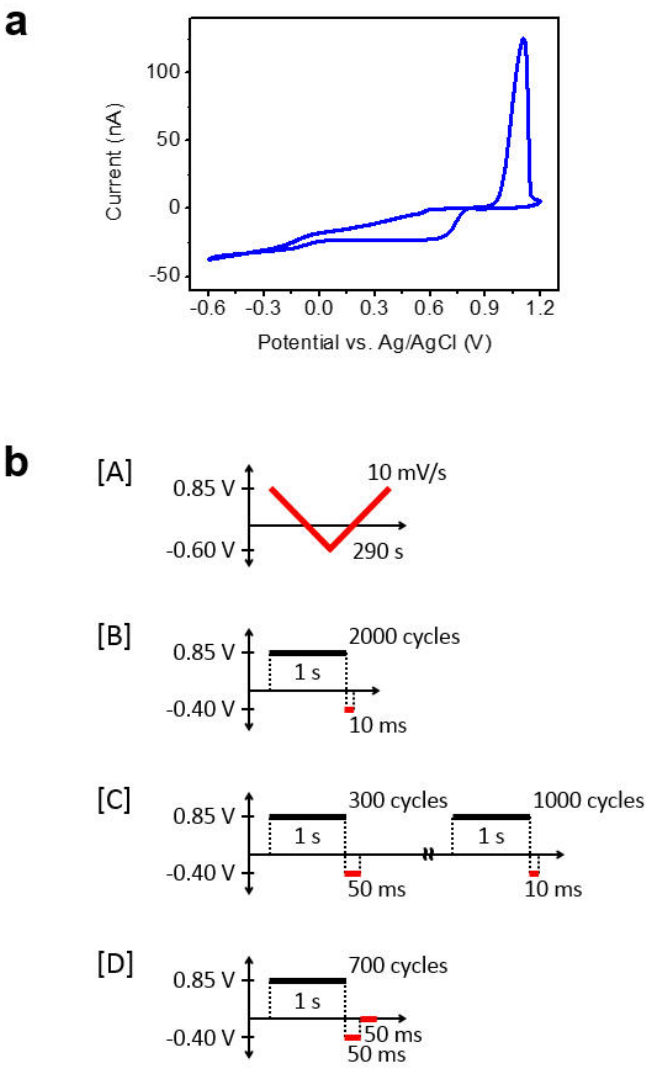


**Fig 3-3** (a) Cyclic voltammogram for the electrodeposition and oxidation of Au on a TiN electrode coated with PDK from a solution containing 1 mM $NaAuCl_4$ and 0.2 M $NaClO_4$, at a scan rate 10 mV $s^{-1}$. The potential scan is initiated at +0.85 V (vs. Ag/AgCl) in the cathodic direction. (b) Schematic diagrams for four types of electrodeposition methods; [A] potential scan method for two segments from +0.85 V to -0.6 V at a scan rate of 10 mV $s^{-1}$ using cyclic voltammetry technique; others using multi-potential step techniques, [B] the optimal electrodeposition potential -0.4 V with pulse duration 10 ms for 2000 cycles; [C] the same potential -0.4 V with mixed pulse duration 50 ms and 10 ms for 300 cycles and 1000 cycles, respectively; [D] a mixed pulse potential -0.4 V and 0.0 V with pulse duration 50 ms for 700 cycles.

### 3.3.2 Confirmation of Au electroplated on the MEA

Information on the surface structure and cross-sectional shape of gold according to the types of electrodeposition method was obtained by confocal laser scanning microscopy (CLSM) and field emission-scanning electron microscopy (FE-SEM) observation; the CLSM images observed with laser reflective DIC (Fig. 3-4 (i)) and the FE-SEM images (Fig. 3-4 (ii)) for the surface morphology confirmation were obtained after the electrochemical plating step, and the sectional images (Fig. 3-4 (iii)) were acquired with FE-SEM after additional step of milling by focused ion beam (FIB) instrument.

The surface of TiN, one of the widely used materials for nerve recording electrodes, is known to be porous [22-23]. As shown in the Fig. 3-4a (i), the surface of the PDK coated TiN electrode observed with laser reflective DIC by the CLSM was difficult to directly confirm that it was porous. Unlike the CLSM image, the surface and cross-sectional images observed by the FE-SEM show that the TiN electrode has a densely porous structure with a thickness of about 350 nm and the TiN MEA consisted of three layers of glass, ITO, and TiN as provided by the MEA manufacturer Multi Channel Systems (MCS) (Fig. 3-4a (ii), (iii)).

In the Au-electroplated electrode by Type [A] which is a potential scanning method, gold was electroplated outgrowing to about 50 $\mu$m beyond the limited TiN MEA size of 30 $\mu$m, and also the surface of the electrode was observed brightly, that is certainly different from the bare TiN electrode (on the CLSM image, Fig. 3-4b (i)). As a

result of FE-SEM observation (Fig. 3-4b (ii), (iii)), the gold was electroplated with an average width of a few micrometers and a thickness of about 150 nm. It is considered that this structure, similar in shape to the plate, has been achieved by the continued growth immediately after the nucleation of gold because the reduction potential of Au precursor was consistently applied.

On the other hand, in the cases of the multi-potential pulse plating type [B] to [D], the surface of each Au-TiN electrode was roughly observed with the confocal laser reflective DIC, but the longer the pulse duration, the brighter the electrode surface: as shown in the Fig.3-4c (i) type [B] 10 ms pulse duration, in the Fig. 3-4d (i) type [C] 50 ms and 10 ms mixed pulse duration, and in the Fig. 3-4e (i) type [D] 50 ms pulse duration. More detailed structural differences of the electroplated Au-TiN electrodes were confirmed by FE-SEM observations. It was confirmed that the pulse-plated Au had better adhesion with TiN electrode than the plating by a potential scanning method. The shape of Au plated on TiN coated with PDK varied depending on composition method of pulse duration and mixed potential pulse.

The plated Au by type [B] at -0.4 V using 10 ms pulse duration was shaped with formed sharp nano-islands with a thickness of about 400 nm (Fig. 3-4c (iii)). The coverage of Au uniformly formed inside the TiN electrode was higher than that of type [A], but the exposed TiN region quite remained (Fig. 3-4c (ii), (iii)). As can be seen in Fig. 3-4d (ii), (iii) and Fig. 3-4e (ii), (iii), the gold, which was

electrochemically plated by type [C] at −0.4 V using 50 ms next 10 ms the mixed−duration of pulse and by type [D] at mixed−potential of −0.4 V and 0.0 V using 50 ms pulse duration, was observed to have a very uniform roughness similar to the porous structure and a thickness of about 200 nm.

Therefore, for the purpose of preparing postsynaptic electrode, we electrochemically plated Au on the TiN MEA by selecting types [C] or [D] methods. Fig. 3−5a indicates the current response detected according to applied the potential pulse for one electroplating cycle. By appropriately applying the conditions of the potential pulse technique at −0.4 V using 50 ms duration, the gold was electrochemically formed to a high coverage on the PDK coated TiN electrode and had the porously rough surface that increased the real surface area. We confirmed the increased real surface area by conducting the cyclic voltammetry in 0.5 M sulfuric acid ($H_2SO_4$) solution. Fig. 3−5b shows the cyclic voltammograms obtained for bare TiN (black line), TiN coated with PDK (blue line), and Au electroplated on TiN coated with PDK (red line). Each voltammogram of TiN and PDK coated TiN electrodes shows little electrochemical behaviors at the applied potential range from 0.0 V to 1.2 V. The non−reactive voltammogram is a characteristic of the inert TiN surface known as a chemically stable conductor. On the contrary, the voltammogram for Au plated TiN is typical of that gold electrode that distinctly presented the anodic peak for the formation of gold oxide and the cathodic peak for the reduction of the formed oxide. On the

anodic sweep starting from 0.0 V, the formation of gold surface oxide is observed. On the reverse scan, the oxide is removed at about +0.4 V to generate a stripping peak. Here from, integration of the current related to reduction peak of the gold surface oxide gives a value of 0.02708 $\mu$C, that this value has been inherently associated with the electrochemically accessible gold surface area. As is known in the literature, the charge required to reduce a monolayer of gold oxide at a polycrystalline surface is 400 $\mu$C $cm^{-2}$ [24]. Thus the real surface area of the electrodeposited gold can be calculated to be 6.77 $\times$ $10^{-5}$ $cm^2$, and the roughness factor is 9.6: it is a calculated value when compared to the geometrical area of the TiN electrode 7.06 $\times$ $10^{-6}$ $cm^2$. By electrochemically plating Au on TiN MEA coated with PDK, the following advantages can be achieved in accordance with the purpose of this study: large surface area, low electrode impedance, enhanced the signal-to-noise ratio (SNR), and easy functionalization with biomolecules.

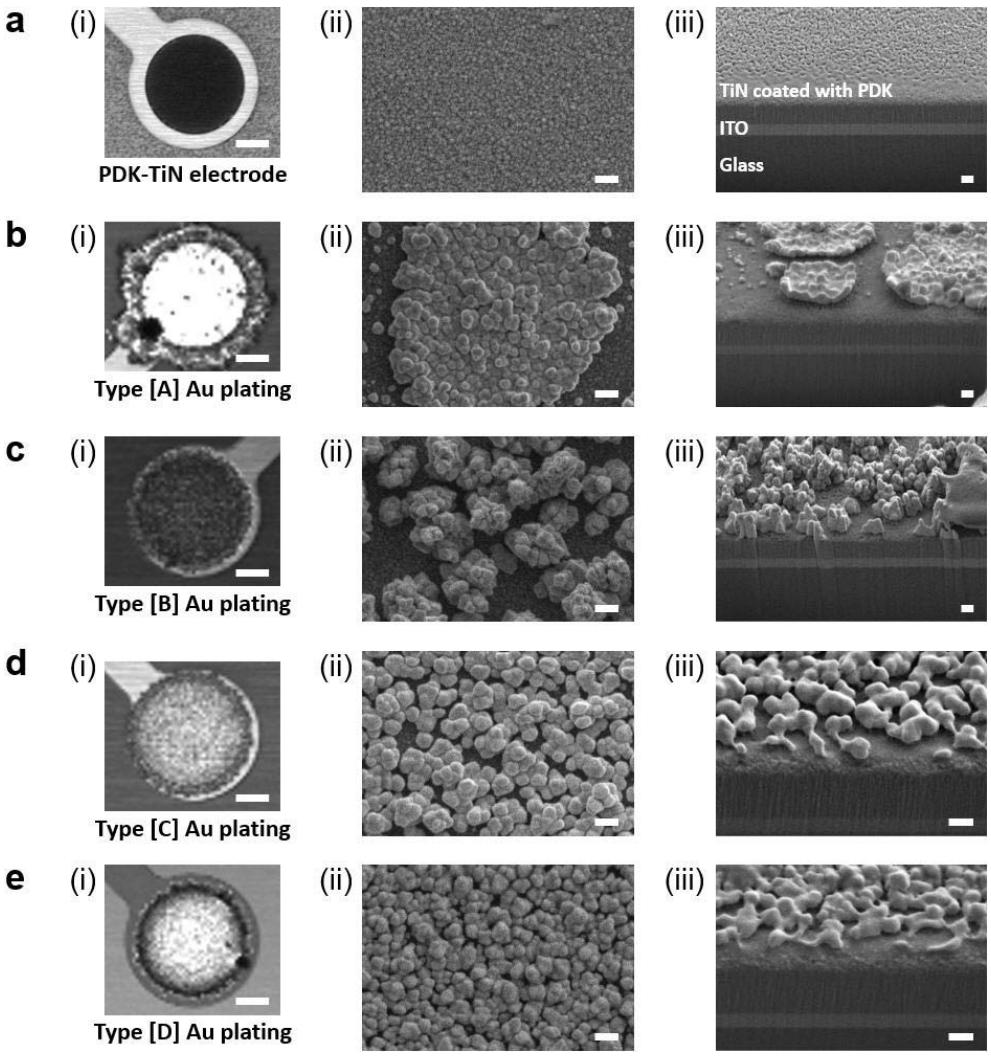


**Fig 3-4** Representative microscope images of TiN electrode coated with PDK and electrochemically plated Au on the TiN electrodes by methods of four types as shown in Fig. 3-3; (a) a TiN electrode coated with PDK; others, Au plated electrodes using methods of (b) type [A], (c) type [B], (d) type [C], and (e) type [D]. (a - e, (i)) show laser reflective DIC images by confocal microscope. Scale bar = 10 $\mu$m. (a - e, (ii)) and (a - e, (iii)) show the FE-SEM images of surface and cross-section for electrodes, respectively. Scale bar = 200 nm.

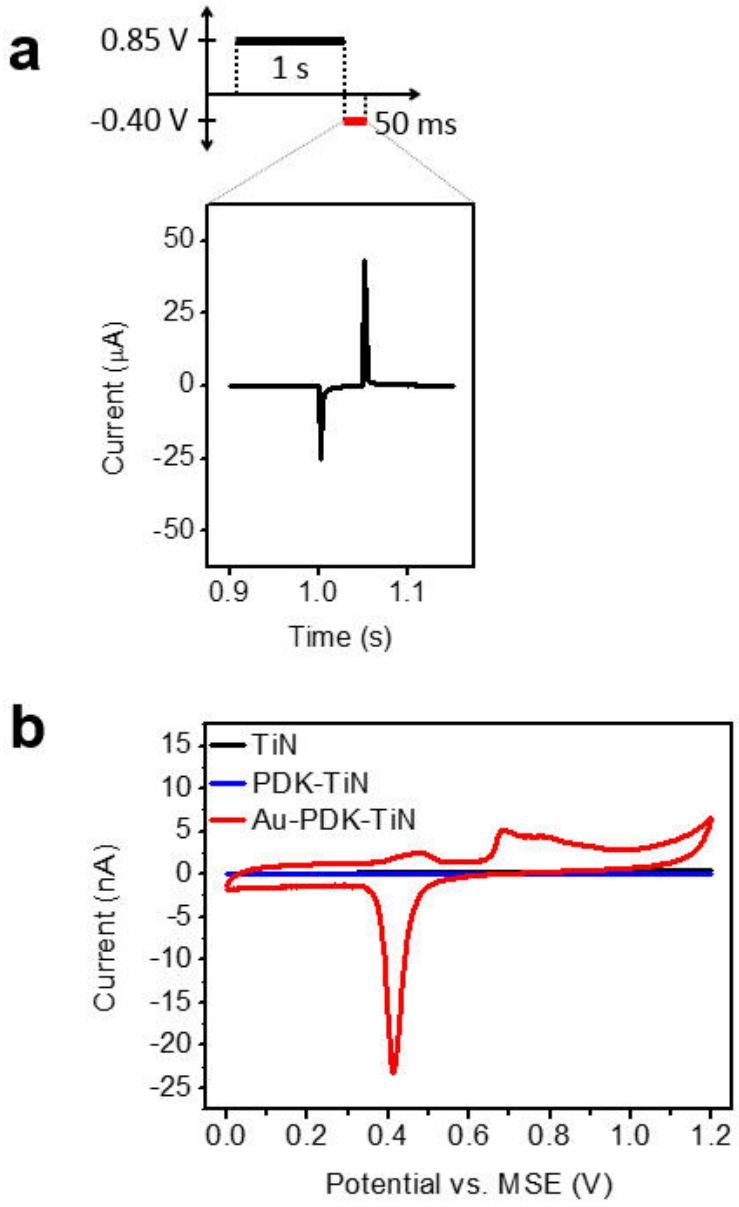


**Fig 3-5** (a) Current response recorded by applying the potential pulse for one cycle of electroplating at −0.4 V (vs. Ag/AgCl) using 50 ms pulse duration. (b) Cyclic voltammograms for a bare TiN (black line), a TiN coated with PDK (blue line), and Au electroplated TiN electrode (red line) in a 0.5 M $H_2SO_4$ solution, at a scan rate 50 mV $s^{-1}$.

### 3.3.3 Electrochemical characterizations of the electrode until Au electroplating process

In order to comprehend the Au-TiN electrode, we performed a study of electrochemical characterization from the bare TiN electrode to the Au electrodeposition on TiN coated with PDK step by step using cyclic voltammetry (CV) and electrochemical impedance spectroscopy (EIS). First, we examined TiN electrode and PDK coated TiN electrode in a solution containing 1 mM $K_3Fe(CN)_6$. Fig. 3-6a shows the voltammograms for the reduction of $[Fe(CN)_6]^{3-}$ on TiN (black line) and PDK coated TiN (blue line) electrode. In the case of TiN electrode, the reductive current of $[Fe(CN)_6]^{3-}$ on scanning the negative potential started from 0.4 V flowed, but the steady-state current, known as a characteristic of the semi-infinite diffusion on ultramicroelectrode, was not observed. We tried this experiment several times, but the results were reproducibly observed without the limiting current (data not shown). This is presumably because the charging current of the TiN electrode is much larger than the reduction current of $[Fe(CN)_6]^{3-}$. After PDK coating on the TiN electrode, the voltammetric curve was completely reduced owing to an insulating effect of PDK. In comparison to the bare TiN, the Nyquist plot on the PDK coated TiN indicated that the electrode impedance was seriously increased and an electron transfer was hindered (Fig. 3-6b). The electrochemically reductive behavior of $[Fe(CN)_6]^{3-}$ on the PDK-TiN electrode seems not to

occur almost, but it is not. As shown in the inset of Fig. 3-6a, the current level was reduced by more than 30 times, but the reduction of $[Fe(CN)_6]^{3-}$ apparently became. We regarded that the coated PDK, which is positively charged amino acid polymer, was not densely packed enough to completely block the surface of TiN electrode and allowed the negatively charged $[Fe(CN)_6]^{3-}$ to easily access the electrode surface due to charge-charge interaction.

To verify this charge effect of the PDK coating, we investigated the reduction behavior of $[Ru(NH_3)_6]^{3+}$ with opposite charge. Similar to the previous step, CV and EIS were conducted in a solution of 1 mM $Ru(NH_3)_6Cl_3$ and then compared with data of $[Fe(CN)_6]^{3-}$. In order to relatively compare the current magnitudes measured by CV, we obtained the voltammograms and corrected the data as follows; we first obtained the voltammograms in only PBS buffer without the redox species, and then in presence of the redox species. Next, we subtracted the charging current taken in the buffer from the voltammograms taken in redox species. Lastly, the voltammogram of $[Fe(CN)_6]^{3-}$ was calibrated by the limiting current value of $[Ru(NH_3)_6]^{3+}$, and then plotted together as in Fig. 3-7a. The electrochemical reduction behavior of positively charged $[Ru(NH_3)_6]^{3+}$ was measured as a slightly lower current value than of $[Fe(CN)_6]^{3-}$ with a negative charge. This may be because the approach of $[Ru(NH_3)_6]^{3+}$ to the TiN electrode was inhibited by the same charged PDK layer. Likewise as shown in the Nyquist plot, the PDK coated TiN electrode impedance was observed lower in a

solution of $[Fe(CN)_6]^{3-}$ (Fig. 3-7b). As a result, this implies that electrochemical deposition using a negatively charged Au precursor ($AuCl_4^-$) can be performed on a positively charged PDK-TiN MEA.

Fig. 3-6c and 3-6d show the voltammograms and the Nyquist plot obtained in the $[Fe(CN)_6]^{3-}$ solution for the electrochemical characterization on the electroplated gold electrode in comparison of PDK coated TiN electrode. The voltammogram on the Au plated PDK-TiN electrode shows the expected electrochemical behavior for the reduction of $[Fe(CN)_6]^{3-}$, which the steady-state current was indicated (Fig. 3-6c red line); by gold, the electrochemical activity of the electrode was greatly improved in compared to the previous electrodes. And the Nyquist plot gained on the Au-PDK-TiN electrode also shows that the significantly lower electrode impedance and increased capacitance were acquired (Fig. 3-6d red line). Consequently, by electroplating gold, it can be seen that the electrochemical electrode activity is enhanced much more than the PDK coated TiN electrode generally used in the neuroscience field.

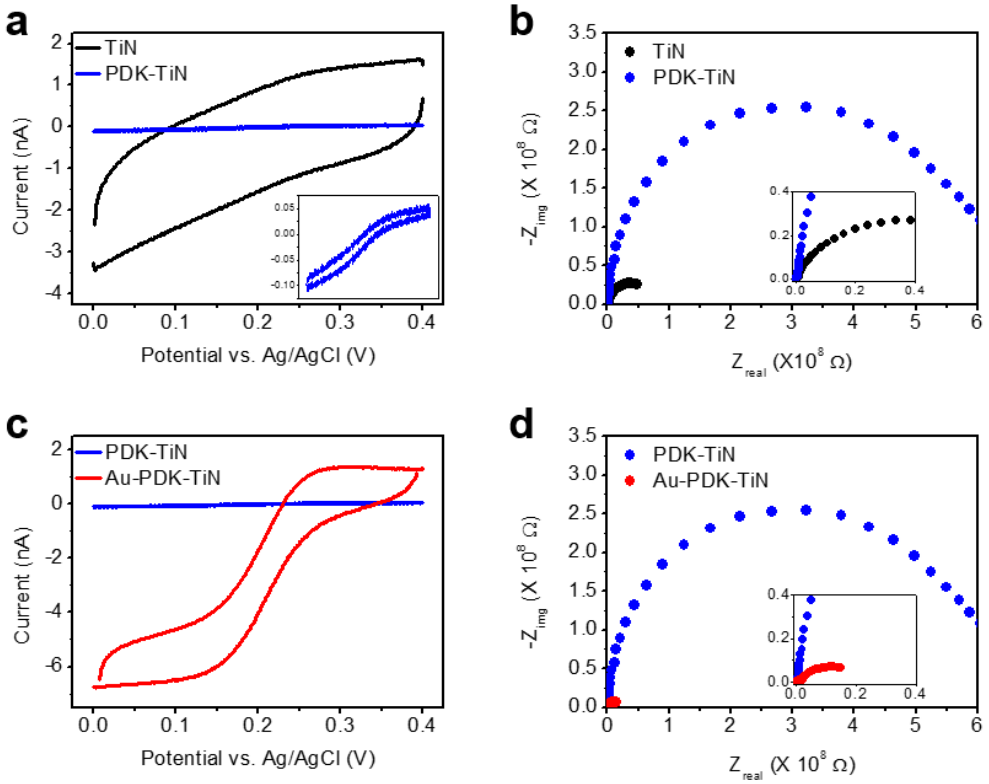


**Fig 3-6** Electrochemical characterizations from a bare TiN electrode to Au electroplating step by step. All data obtained in a solution of 1 mM $K_3Fe(CN)_6$ in PBS (pH 7.0). (a, c) The voltammograms recorded by cyclic voltammetry (CV), at a scan rate 50 mV $s^{-1}$ and (b, d) the Nyquist plots recorded by electrochemical impedance spectroscopy (EIS), at the applied DC potential +0.2 V (vs. Ag/AgCl); (a, b) comparison of bare TiN and PDK coated TiN electrodes and (c, d) comparison before and after Au plating on the PDK-TiN.

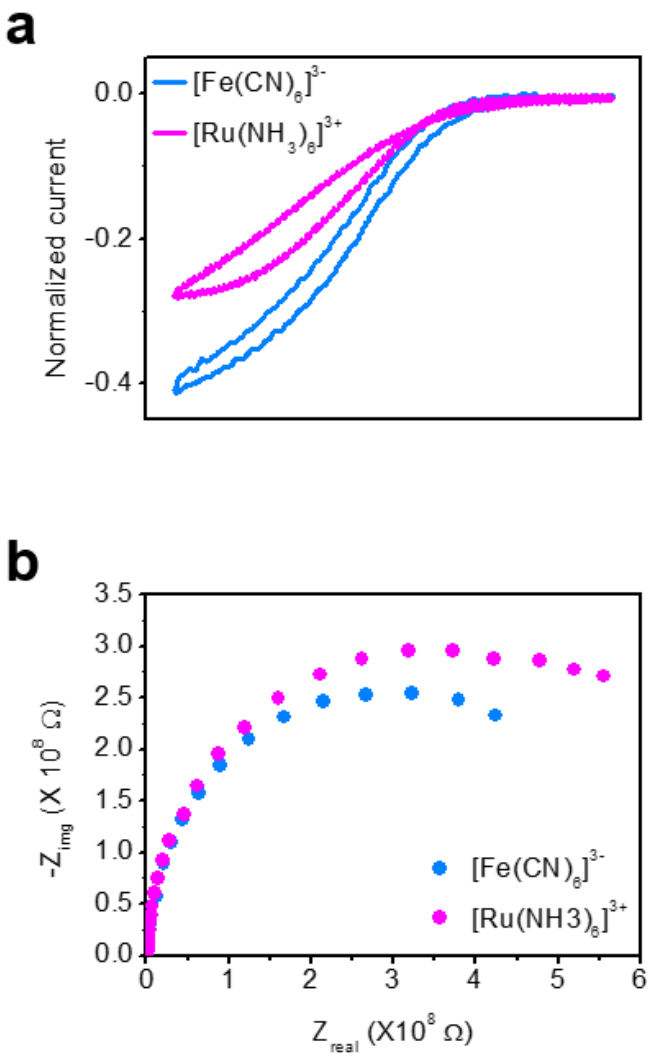


**Fig 3-7** Electrochemical characterizations in order to confirm the electro-activity of PDK coated TiN electrode and the charge effect by PDK. Comparison of data between redox molecules with opposite charge after recorded in condition of 1 mM $K_3Fe(CN)_6$ in PBS and 1 mM $Ru(NH_3)_6Cl_3$ in PBS, respectively. (a) Normalized cyclic voltammograms at a scan rate of 50 mV $s^{-1}$. (b) Nyquist plots at the applied DC potential +0.2 V (vs. Ag/AgCl) in 1 mM $K_3Fe(CN)_6$ and the applied DC potential -0.2 V (vs. Ag/AgCl) in 1 mM $Ru(NH_3)_6Cl_3$, respectively.

### 3.3.4 Surface modification for fabrication of the postsynaptic electrode

To fabricate a postsynaptic electrode in earnest on Au electroplated PDK-TiN MEA, we proceeded step-by-step to the surface modification process to finally immobilize the postsynaptic CAM. As mentioned in the experimental section, we formed a self-assembled monolayer (SAM) molecule containing thiol head group and biotin functional group on the surface of the electrode after electrodeposition of gold. And then the streptavidin with four binding sites having an extraordinarily high affinity for biotin was introduced on the biotin-SAM formed Au-PDK-TiN MEA. Because the binding of biotin to streptavidin having the dissociation constant ($K_d$) of ~ $10^{-14}$ mol/L is known as one of the strongest non-covalent interactions, streptavidin would stably retain conjugation between the biotin-SAM formed electrode and a NL1-R as a postsynaptic CAM to be finally immobilized. After NL1-R immobilization, laminin with low concentration enough to aid cell adhesion on the MEA was additionally treated for the purpose of stable neuronal cell culture. When laminin was not treated, neurons sometimes developed abnormally or did not grow at all. Therefore, by treating laminin before primary neuronal cell culture, the cells grew normally and healthy, and then artificial synapses were also stably induced on the postsynaptic electrode. As shown in Fig. 3-8a, half of 59 electrodes aligned in 6 x 6 layout grid in the MEA were electrochemically plated

with gold and the electrode surface modification process was performed up to immobilization of the NL1-R. Fig. 3-8b and 3-8c, which are imaged observed with CLSM after the end of the surface modifications, show the laser reflected DIC image of Au plated MEA and fluorescence image for RFP of immobilized NL1-R, respectively. As a result, we selectively plated the gold to the desired electrode among the MEA electrodes, and were able to effectively immobilize NL1-R only on that electrodes.

As the surface modification proceeds step-by-step, it was confirmed how the electrochemical behavior of the electrode changes through conducting the CV and EIS in a solution of containing 1 mM $K_3Fe(CN)_6$ similar to previous electrochemical characterization experiments. The voltammograms show that the reduction current of $[Fe(CN)_6]^{3-}$ gradually decreased every time the step of the modification was added, and the electrode impedance eventually increased as shown in the Nyquist plot (Fig. 3-9a and 3-9b). However, the electrochemical behavior on the postsynaptic electrode is not impossible at all. Thereby after the immobilization of biomolecules the reduction behavior of $[Fe(CN)_6]^{3-}$ was observed in the voltammograms and electron transfer kinetics was seen in the Nyquist plot, the postsynaptic electrode would have activity sufficiently to record neural information or identify electrochemical behaviors in synaptic cleft via formed the artificial synaptic interface.

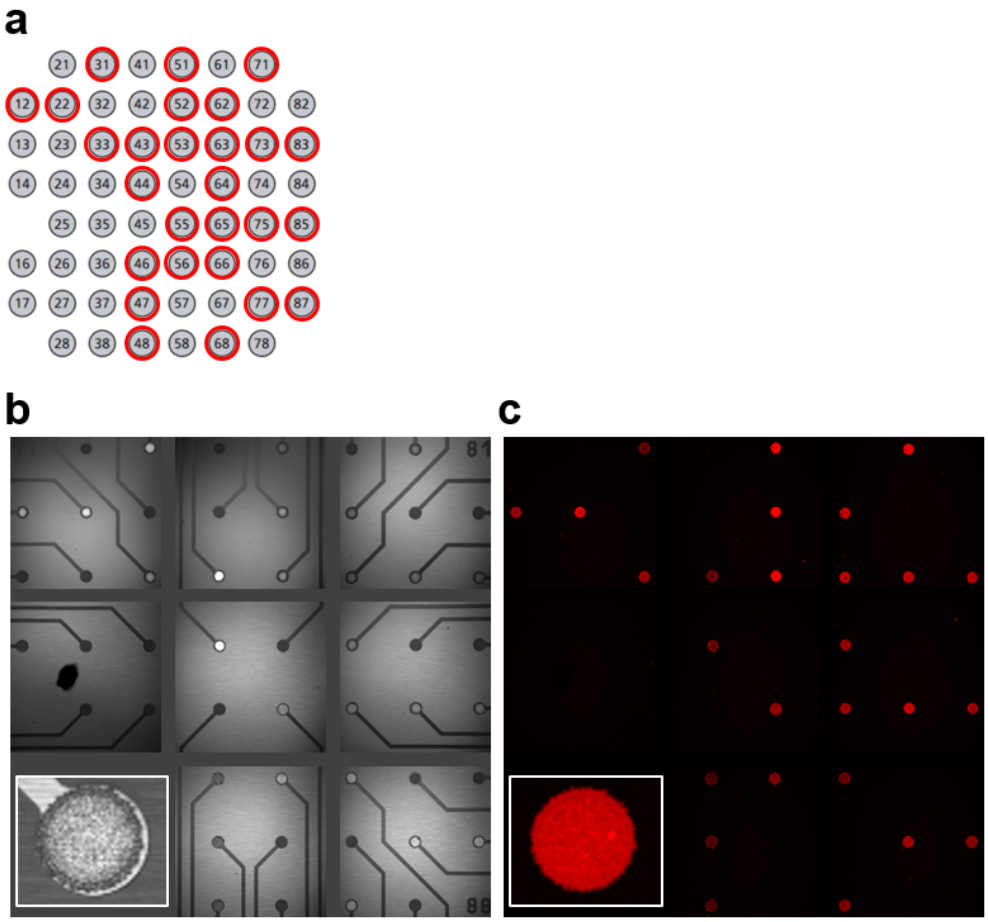


Fig 3-8 (a) The MEA layout; red circles indicate the position of gold (Au) electroplated electrodes. (b, c) Confocal microscope images observed after electrodeposition of Au and the surface modification with the biotinylated postsynaptic CAM, NL1-R; (b) laser reflective DIC images and (c) fluorescence images for RFP of NL1-R immobilized on the electrodes: inset images are enlarged images for one of them, respectively.

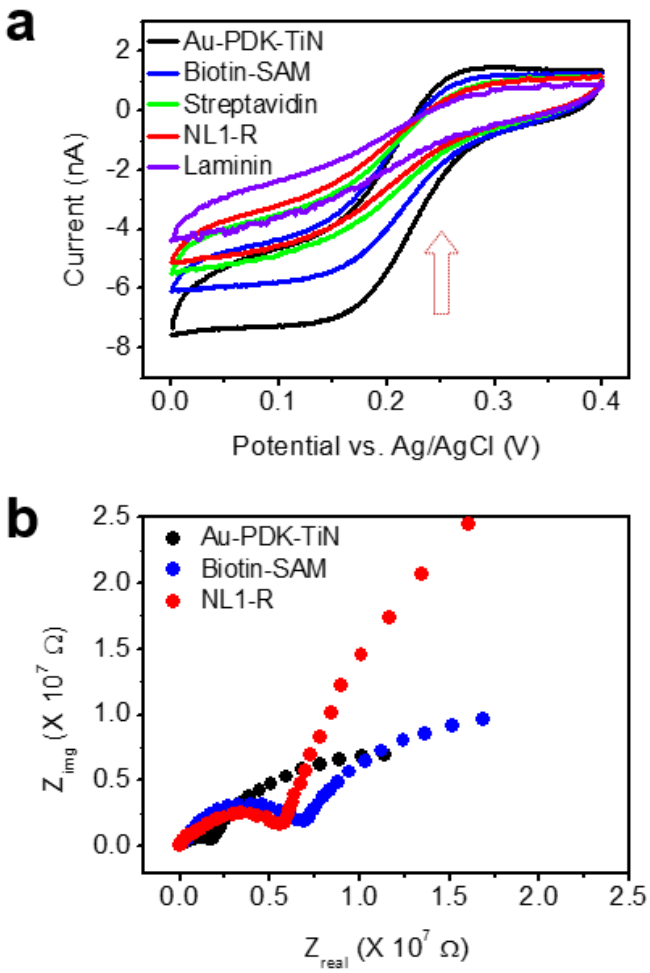


**Fig 3-9** Confirmation of electrochemical behaviors for each surface modification process for the postsynaptic electrode fabrication. All data obtained in a solution of 1 mM $K_3Fe(CN)_6$ in PBS (pH 7.0). (a) Cyclic voltammograms recorded depending on the surface modification step with a scan rate of 50 mV $s^{-1}$; Au plated PDK-TiN electrode (black), formation of biotin-SAM (blue), immobilization of streptavidin (green), immobilization of NL1-R (red), and additional coating of laminin (violet). (b) Nyquist plots of the impedance data recorded by the applied DC potential +0.2 V (vs. Ag/AgCl); Au plated PDK-TiN electrode (black), formation of biotin-SAM (blue), and finally immobilization of NL1-R (red).

### 3.3.5 Artificial synapses induced between neurons and the postsynaptic electrodes

We cultured rat primary hippocampal neurons on the MEA containing the postsynaptic electrodes for 14 DIV (days *in vitro*). To confirmation of the artificial hemisynapse induced on the postsynaptic electrodes we accomplished immunocytochemistry (ICC), and the excitatory glutamatergic presynapses differentiated by NL1-R was identified using an anti-VGlut1 (vesicular glutamate transporter 1) antibody. Fig. 3-10a shows the merged image with the presynaptic marker synapsin I (syn I), the excitatory presynaptic marker VGluT1 and DIC indicating the position of the electrode. Fig. 3-10b and 3-10c show that the electrodes with artificial synapses indicated by the arrows in Fig.3-10a, respectively. As a result of observation by FE-SEM (Fig 3-10b (i) and Fig. 3-10c (i)), the neurites grew and maintained as much contact as possible with the postsynaptic electrodes. We found that the postsynaptic electrodes immobilized with NL1-R successfully induced excitatory presynaptic differentiation, showing much higher immunoreactivity to syn I (green color) and VGluT1 (red color) than the outer part of the electrodes or non-postsynaptic electrodes (Fig. 3-10b (ii) and Fig. 3-10c (ii)). Currently, we are continuously conducting to electrochemically detect the neurotransmitter glutamate released via the artificial synapse formed on the postsynaptic electrode, and the research on this part is ongoing in several ways including

potentiometry, impedometry, and optical detection using the engineered glutamate sensor protein iESF.

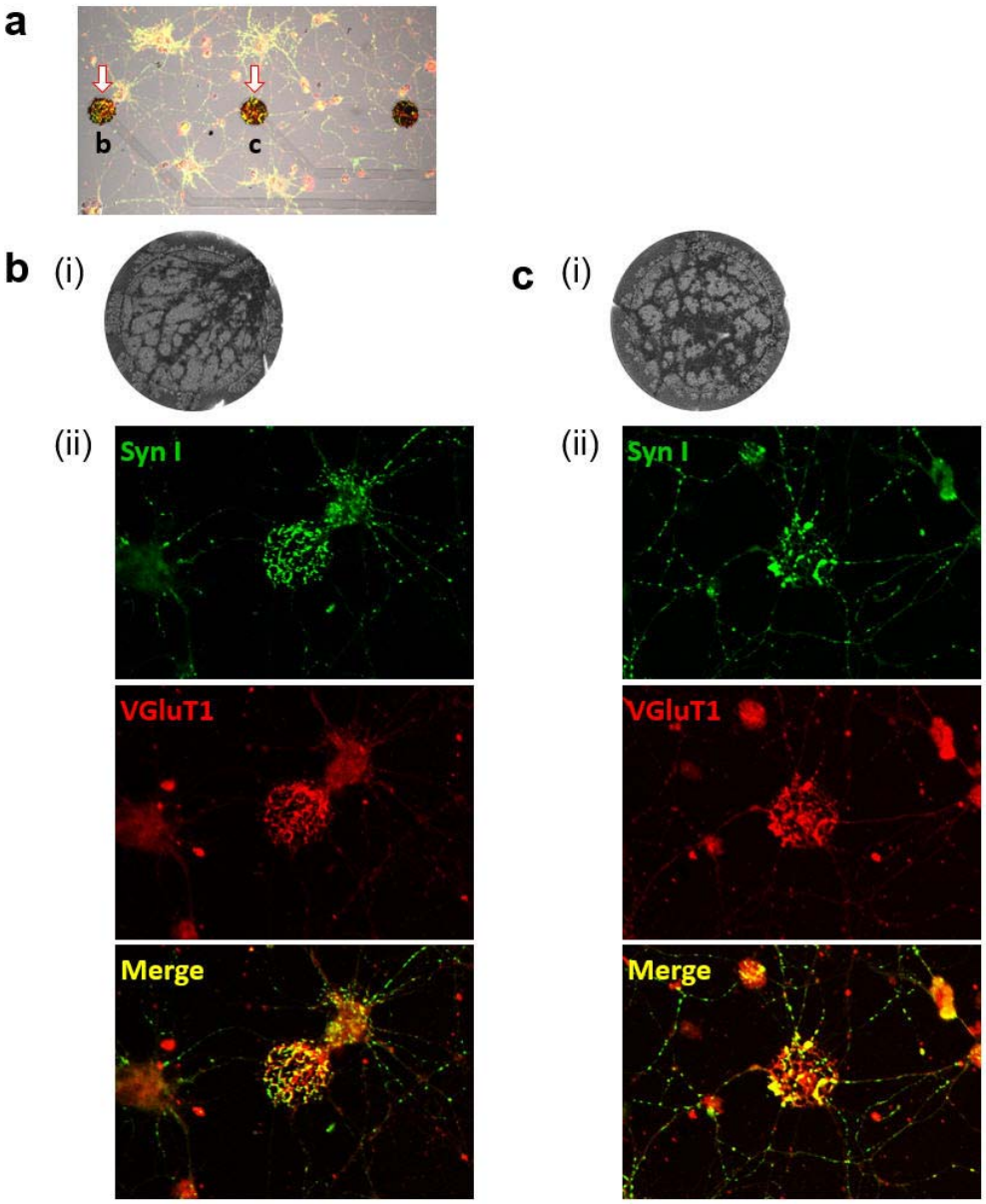


Fig 3-10 Immunocytochemistry (ICC) mages for the artificial synapses induced on the chemically modified hybrid postsynaptic electrode. (a) Merged images with DIC image and fluorescence images for antibodies of target marker proteins by confocal microscope; the arrows indicate the induced artificial synapses on the electrodes and the position of them are magnified in (b) and (c), respectively; ((i) in b, c) FE-SEM images and ((ii) in b, c) each images doubly stained by anti-synapsin I (syn I, green) and anti VGluT1 (red) and merged images by confocal microscope.

## 3.4 Conclusion

In this study, we propose an artificial synaptic interface to be active neural interface based on synapse and report for replacing the postsynaptic neurons that receive the neural signals with the modified microelectrodes. This is an unprecedented new approaching strategy in the field of neural interfaces. By electrochemically plating gold on a commercially available TiN MEA coated with PDK using a multi-potential pulse technique, the electrochemical activity of the electrode was improved with large surface area, low electrode impedance, and easy surface functionalization with biomolecules. The postsynaptic CAM NL1-R was finally immobilized on the electrode in order to fabricate the postsynaptic electrodes capable of inducing the artificial synapses, thus the type-specific and durable glutamatergic artificial presynapses were formed to the neurons contacting on the postsynaptic electrodes. With this system, we currently tried to monitor neurotransmitters as well as electrical signal through the artificial synapses. Contrary to directly physical contact between biological neuronal cells and bare electrodes, the proposed system of the artificial synapse provide new platform of neural interfaces and we expect that it can be possible to directly detect meaningful synaptic signals and to bilaterally communicate to neuron with regulating spatiotemporal feedback.

## 3.5 References

[1] P. Fattahi, G. Yang, G. Kim and M. R. Abidian, *Adv. Mater.*, 2014, *26*, 1846.

[2] J. R. Wolpaw, N. Birbaumer, D. J. McFarland, G. Pfurtscheller and T. M. Vaughan, *Clin. Neurophysiol.*, 2002, *113*, 767.

[3] M. A. Lebedev and M. A. L. Nicolelis, *Trends Neurosci.*, 2006, *29*, 536.

[4] J. R. Wolpaw and D. J. McFarland, *Proc. Natl. Acad. Sci.* 2004, *101*, 17849.

[5] L. R. Hochberg, D. Bacher, B. Jarosiewicz, N. Y. Masse, J. D. Simeral, J. Vogel, S. Haddadin, J. Liu, S. S. Cash, P. van der Smagt and J. P. Donoghue, *Nature*, 2012, *485*, 372.

[6] C. Ribrault, K. Sekimoto and A. Triller, *Nat. Rev. Neurosci.*, 2011, *12*, 375.

[7] H. Hu, J. Gan, and P. Jonas, *Science*, 2014, *345*, 529.

[8] Y.-T. Li, S.H. Zhang, X.-Y. Wang, X.-W. Zhang, A. Oleinick, I. Svir, C. Amatore and W.-H. Huang, *Angew. Chem. Int. Ed.*, 2015, *54*, 1.

[9] R. M. Wightman, J. A. Jankowski, R. T. Kennedy, K. T. Kawagoe, T. J. Schroeder, D. J. Leszczyszyn, J. A. Near, Jr., E. J. Diliberto and O. H. Viveros, *Proc. Natl. Acad. Sci.* 1991, 88, 10754.

[10] ) X. Zhu, Y. Qiao, X. Zhang, S. Zhang, X. Yin, J. Gu, Y. Chen, Zhu, Z. M. Li and Y. Shao, *Anal. Chem.*, 2014, *86*, 7001.

[11] P. Actis, S. Tokar, J. Clausmeyer, B. Babakinejad, S. Mikha-

leva, R. Cornut, Y. Takahashi, A. Lpez Crdoba, P. Novak, A. I. Shevchuck, J. A. Dougan, S. G. Kazarian, P. V. Gorelkin, A. S. Erofeev, I. V. Yaminsky, P. R. Unwin, W. Schuhmann, D. Klenerman, D. A. Rusakov, E. V. Sviderskaya and Y. E. Korchev, *ACS Nano*, 2014, *8*, 875.

[12] Y. T. Li, S. H. Zhang, L. Wang, R. R. Xiao, W. Liu, X. W. Zhang, Z. Zhou, C. Amatore and W. H. Huang, *Angew. Chem. Int. Ed.*, 2014, *53*, 12456; *Angew. Chem.* 2014, *126*, 12664.

[13] E. J. Kim, C. S. Jeon, S. Y. Lee, I. Hwang and T. D. Chung, *Sci. Rep.*, 2016, *6*:24210.

[14] P. V. Dudin, P. R. Unwin and J. V. Macpherson, *J. Phys. Chem. C*, 2010, *114*, 13241.

[15] P. V. Dudin, M. E. Snowden, J. V. J. V. Macpherson and P. R. Unwin, *ACS Nano*, 2011, *5*, 10017.

[16] L. Komsiyska and G. Staikov, *Electrochim. Acta*, 2008, *54*, 168.

[17] G.J. Brewer, J.R. Torricelli, E.K. Evege and P.J. Price, *J. Neurosci. Res.*, 1993, *35*, 567

[18] C. M. Hales, J. D. Rolston and S. M. Potter, *J. Vis. Exp.*, 2010, *39*, e2056

[19] H. Martin, P. Carro, A. H. Creus, S. Gonzales, R. C. Salvarezza and A. J. Arvia, *Lanmuir*, 1997, 13, 100.

[20] A. D. Goolsby and D. T. Sawyer, *Anal. Chem.*, 1968, 40, 1978.

[21] J. E. Anderson and S. M. Sawtelle, *Inorg. Chim. Acta*, 1992, 194, 171.

[22] S. F. Cogan, *Annu. Rev. Biomed. Eng.*, 2008, *10*, 275.

[23] S. A. G. Evans, J. G. Terry, N. O. V. Plank, A. J. Walton, L. M. Keane, C. J. Campbell, P. Chazal, J. S. Beattie, T.-J. Su, J. Crain and A. R. Mount, *Electrochem. Commun.*, 2005, *7*, 125.

[24] G. T.-Filho, A. H. Dall' Antonia and G. Jerkiewicz, *J. Electroanal. Chem.*, 2005, *578*, 1.

# 4. Summary and Perspectives

In the neural interface fields, traditional systems for acquiring neural information rely solely on the electrical signals using neural electrodes. However, it is difficult to understand the prior information of the nerve signals in the real brain alone with the electrical signals. This dissertation indicates a new artificial synaptic interface focusing on the actual brain synaptic system, unlike existing neural interface technology. By inducing an artificial synapse between the abiotic electrode and the neuron, a more sophisticated neural interface can be constructed, and not only the electrical signals but also the synaptic chemical signal information can be detected. Furthermore, an electrochemical study via the artificial synapse can be carried out to closely examine the synaptic behavior.

For inducing the artificial synapse with type-specificity, synaptic cell adhesion molecules (synaptic CAMs), which play an important role in determining the specificity, have been engineered with fluorescent protein and biotinylation. In Chapter 2, the engineered postsynaptic CAMs displayed on abiotic solid microbeads can play a role as artificial dendrites, inducing the formation of durable excitatory and inhibitory hemisynapses with spatiotemporal regulation; excitatory synapse by neuroligin 1 (NL1R) and inhibitory synapse by neuroligin 2 (NL2R) and slitrk3 (SL3R). Such robust and type-specific artificial synapse demonstrates a novel platform of neuro-electronic interface that enables information processing via

the synapse, and shows the potential for developing fundamental study on information process of neural networks in the brain.

Research on the synapse has been actively pursued in relation to neurotransmission in the field of neural interface. So far, many studies have attempted to detect neurotransmitters that have spread outside the synapse, or are still systems that rely on the electrical signal detection. In Chapter 3, an active neural interface based on the artificial synapse between the electrode and neuron has been constructed by replacing the postsynaptic neuron that receive the neural information with the surface-modified microelectrode. In order to modify the surface of the electrode for inducing the artificial synapse, commercially available electrodes were first electrochemically plated with gold, and then followed by process of surface functionalization to finally immobilize the postsynaptic CAM NL1R. Consequently, the electrochemical activities of the electrode, such as the increase of the surface area of the electrode and the decrease of the interfacial resistance, were improved, and the durable artificial presynapses with type-specificity were differentiated to the neurons contacting on the modified electrodes. Based on the artificial synaptic interface, this system will be able to distinguish meaningful synaptic signals from complex neural information by monitoring the behavior of neurotransmitters released into the synapse, and also bilaterally communicate to neuron with regulating spatiotemporal feedback. Moreover, it is expected that basic research on the neurotransmission process through artificial

synapse will be possible by electrochemical study in the artificial synaptic cleft which is a uniform and complicated bio-electronic nanogap.

# 국문초록

최근 전세계적으로 뇌와 신경계에 대한 사회적인 관심 증가와 함께 브레인-컴퓨터 인터페이스 (brain-computer interface, BCI)와 뇌역공학 (reverse engineering the brain)과 같은 신경 인터페이스 분야의 연구가 활발히 이루어지고 있다. 신경 인터페이스는 생체 내 신경계와 외부 바깥 세상을 기기 장치로 연결하여 신경 정보를 얻거나 신경 네트워크를 이해하는데 주된 목적을 두고 있다. 대부분의 신경 인터페이스 기술은 신경계 조직 혹은 세포 근처에 신경 전극 (neural electrodes)을 단순히 위치시킴으로써 전극과 신경계와의 매우 수동적이고 물리적인 접촉에만 의존하고 있다. 실제 신경생물학적 체계에서 신경세포들은 시냅스라는 세포 접합 부위를 통해 전기적인 신호인 활성전위 (action potentials, APs)와 화학적인 신호인 신경전달물질 (neurotransmitters)의 형태로 신경 정보를 전달함으로써 서로 긴밀한 의사소통을 한다. 신경정보전달 조절의 중요한 역할을 하는 시냅스는 신호를 전달하는 흥분성 시냅스 (excitatory synapse)와 신호 전달을 저지하는 억제성 시냅스 (inhibitory synapse)로 구분된다. 이런 시냅스의 특이성을 결정하는 데에는 신경접착분자 (synaptic cell adhesion molecules, synaptic CAMs) 단백질들이 중요한 핵심 요인이며, 이들은 시냅스를 이루고 있는 두 신경세포의 세포막에 위치하여 서로 쌍을 이루어 접합함으로써 매우 좁은 약 20 nm 의 시냅스 틈새 (synaptic cleft)를 유지한다. 이와 같은 시냅스 시스템에 초점을 두어, 본 학위논문에서는 전극과 신경세포 사이에 인공시냅스 인터페이스를 구축함으로써 인공시냅스로 연결하는 새로운 신경 인터페이스의 플랫폼을 제안한다. 인공시냅스를 통해 시냅스 기반

신경정보를 검출함으로써 신경세포와의 양방향 의사소통이 가능할 것이며, 인공시냅스에 의해 형성된 매우 좁은 나노 틈새 (synaptic cleft)에서의 신경신호 거동에 대한 새로운 전기화학적 연구를 수행할 수 있을 것이라 기대한다. 시냅스 특이성과 견고성을 가진 인공시냅스 인터페이스를 구축하기 위하여, 전극의 표면 개질화에 조작된 신경접착단백질을 도입하는 일련의 연구들을 수행하였다.

먼저, 조작한 시냅스후 접착단백질 (postsynaptic CAMs)을 마이크로비드에 기능화한 인공수상돌기 (artificial dendrites)에 의해 견고하게 시냅스 특이성을 갖는 인공시냅스가 유도됨을 확인하였다. 흥분성과 억제성의 시냅스 특이성은 신경 네트워크 안에서 화학적인 신경전달물질을 통한 신경정보 처리를 조절하는 기능을 한다. 시냅스 기반 신경 인터페이스에 기초를 두기 위해, 특이성-시냅스생성 단백질 엑토도메인 (ectodomain)의 C-말단에 형광단백질 (red fluorescent protein, RFP)과 바이오틴 (biotin)이 표지되도록 조작하였고, 이를 인공물인 마이크로비드에 기능화 해줌으로써 인공수상돌기를 준비하였다. 흥분성 인공시냅스는 조작한 neuroligin 1 (NL1-R)에 의해 유도 가능했고, 신경세포와 함께 배양함으로써 세포분화단계에 상관없이 세포에 흥분성 시냅스전 분화를 형성시켰다. 억제성 인공시냅스는 neuroligin 2 (NL2-R)와 slitrk3 (SL3-R)에 의해 유도 가능했으며, 성체 신경세포와 함께 배양해줌으로써 신경세포에 억제성 시냅스전 분화를 생성시켰다. 마이크로유체 배양 챔버 (microfluidic culture chamber) 시스템을 이용하여 신경세포의 축색돌기 (axons)를 세포체 소마 (somata)와 수상돌기 (dendrites)로부터 분리하여 배양한 뒤, 인공수상돌기인 시냅스후 접착단백질 마이크로비드와 신경세포의

축색돌기와 접촉함으로써 인공시냅스가 단백질에 따라 시냅스 특이성을 유지한 채 견고하게 유도되었다. 또한 형성된 인공시냅스에서, 특히 NL1-R 에 의한 흥분성 인공시냅스에서 신경전달물질인 글루타메이트(glutamate)가 세포 자극에 의해 방출되는 것을 검출함으로써 유도한 인공시냅스가 활성을 지닌 시냅스임을 확인하였다. 견고하게 시냅스 특이성을 유지하면서 활성을 갖는 인공시냅스는 시냅스 기반 인터페이스 구축으로의 가능성을 보여줬다.

둘째, 상용화된 마이크로전극 어레이 (microelectrode array, MEA)를 이용하여 전극에 금을 전기화학적으로 도금하고 조작한 시냅스후 접착단백질 NL1-R 을 고정해줌으로써 전극과 접촉한 신경세포에 인공시냅스를 유도하였다. 다중 전압 펄스 방법 (multi-potential pulse technique)을 이용하여 전극 위에 금을 전기화학적으로 도금함으로써 전극 표면에 균일하게 금이 도금되었고 거칠기 (roughness)를 가진 구조를 함으로써 전극 실제 표면적이 증가하였고 낮은 전극 계면 저항을 나타냈다. 금을 도금함으로써 일반적으로 사용되는 폴리라이신 폴리머를 코팅한 마이크로전극 (poly-D-lysine, PDK coated MEA) 보다 향상된 전극의 전기화학적 활성을 보여주었고, 또한 금이 생체친화성 금속이면서 표면 기능화가 쉬운 금속이라는 이점을 활용할 수 있었다. 전극에 금을 도금한 후에 바이오틴이 표지된 싸이올 (thiol) 분자를 이용하여 자가조립단층 (self-assembled monolayer, SAM)을 형성하였고, 스트렙타비딘 (streptavidin, SAV)을 고정한 뒤 조작한 시냅스후 접착단백질 NL1-R 을 최종적으로 고정하였다. 이와 같은 표면 개질화 과정을 통해 시냅스후 전극을 준비하였고, 시냅스후 전극은 충분히 신경신호를 검출하거나 시냅스 틈새 전기화학 연구를 수행할

만큼 전기화학적으로 활성을 가진 전극임을 확인하였다. 게다가 신경세포를 전극 위에 배양함으로써 전극과 접촉한 세포에 흥분성 인공시냅스가 유도됨을 확인하였다. 따라서 인공물인 전극 위에 인공시냅스를 형성할 수 있는 전극을 제작하였고, 인공시냅스 기반 인터페이스를 구축할 수 있음을 확인하였다. 앞으로 인공시냅스 인터페이스를 통한 신경신호 검출 및 신경정보전달의 거동에 대한 새로운 전기화학적 연구가 가능할 것이다.

*핵심단어*: 인공시냅스 인터페이스, 신경접착단백질, 표면 개질화된 전극, 인공시냅스에서의 전기화학
*학번*: 2010-30091